

7-16-2021


Evaluating Irrigation Performance and Water Productivity Using EEFlux ET and NDVI

Usha Poudel
University of Nevada, Las Vegas

Haroon Stephen
University of Nevada, Las Vegas, haroon.stephen@unlv.edu

Sajjad Ahmad
University of Nevada, Las Vegas, sajjad.ahmad@unlv.edu

Follow this and additional works at: https://digitalscholarship.unlv.edu/fac_articles

 Part of the [Sustainability Commons](#), and the [Water Resource Management Commons](#)

Repository Citation



Poudel, U., Stephen, H., Ahmad, S. (2021). Evaluating Irrigation Performance and Water Productivity Using EEFlux ET and NDVI. *Sustainability*, 13(14), 1-26.
<http://dx.doi.org/10.3390/su13147967>

This Article is protected by copyright and/or related rights. It has been brought to you by Digital Scholarship@UNLV with permission from the rights-holder(s). You are free to use this Article in any way that is permitted by the copyright and related rights legislation that applies to your use. For other uses you need to obtain permission from the rights-holder(s) directly, unless additional rights are indicated by a Creative Commons license in the record and/or on the work itself.

This Article has been accepted for inclusion in Civil & Environmental Engineering and Construction Faculty Publications by an authorized administrator of Digital Scholarship@UNLV. For more information, please contact digitalscholarship@unlv.edu.

Article

Evaluating Irrigation Performance and Water Productivity Using EEFlux ET and NDVI

Usha Poudel, Haroon Stephen  and Sajjad Ahmad * 

Department of Civil and Environmental Engineering and Construction, University of Nevada Las Vegas, 4505 S. Maryland Pkwy, Las Vegas, NV 89154, USA; poudeu1@unlv.nevada.edu (U.P.); haroon.stephen@unlv.edu (H.S.)
* Correspondence: sajjad.ahmad@unlv.edu; Tel.: +1-702-895-5456

Abstract: Southern California's Imperial Valley (IV) faces serious water management concerns due to its semi-arid environment, water-intensive crops and limited water supply. Accurate and reliable irrigation system performance and water productivity information is required in order to assess and improve the current water management strategies. This study evaluates the spatially distributed irrigation equity, adequacy and crop water productivity (CWP) for two water-intensive crops, alfalfa and sugar beet, using remotely sensed data and a geographical information system for the 2018/2019 crop growing season. The actual crop evapotranspiration (ET_a) was mapped in Google Earth Engine Evapotranspiration Flux, using the linear interpolation method in R version 4.0.2. The `approx()` function in the base R was used to produce daily ET_a maps, and then totaled to compute the ET_a for the whole season. The equity and adequacy were determined according to the ET_a's coefficient of variation (CV) and relative evapotranspiration (RET), respectively. The crop classification was performed using a machine learning approach (a random forest algorithm). The CWP was computed as a ratio of the crop yield to the crop water use, employing yield disaggregation to map the crop yield, using county-level production statistics data and normalized difference vegetation index (NDVI) images. The relative errors (RE) of the ET_a compared to the reported literature values were 7–27% for alfalfa and 0–3% for sugar beet. The average ET_a variation was low; however, the spatial variation within the fields showed that 35% had a variability greater than 10%. The RET was high, indicating adequate irrigation; 31.5% of the alfalfa and 12% of the sugar beet fields clustered in the Valley's central corner were consuming more water than their potential visibly. The CWP showed wide variation, with CVs of 32.92% for alfalfa and 25.4% for sugar beet, signifying a substantial scope for CWP enhancement. The correlation between the CWP, ET_a and yield showed that reducing the ET_a to approximately 1500 mm for alfalfa and 1200 mm for sugar beet would help boost the CWP without decreasing the yield, which is nearly equivalent to 44.52M cu. m (36,000 acre-ft) of water. The study's results could help water managers to identify poorly performing fields where water conservation and management could be focused.



Citation: Poudel, U.; Stephen, H.; Ahmad, S. Evaluating Irrigation Performance and Water Productivity Using EEFlux ET and NDVI. *Sustainability* **2021**, *13*, 7967. <https://doi.org/10.3390/su13147967>

Academic Editor: Ozgur Kisi

Received: 10 June 2021

Accepted: 13 July 2021

Published: 16 July 2021

Publisher's Note: MDPI stays neutral with regard to jurisdictional claims in published maps and institutional affiliations.



Copyright: © 2021 by the authors. Licensee MDPI, Basel, Switzerland. This article is an open access article distributed under the terms and conditions of the Creative Commons Attribution (CC BY) license (<https://creativecommons.org/licenses/by/4.0/>).

Keywords: EEFlux; irrigation performance; CWP; water conservation; NDVI

1. Introduction

Irrigated agriculture is the major consumer of freshwater supplies, being attributed to 65% of total water withdrawals [1,2]. With a rising population, the demand for food production is growing, whereas the share of irrigation water for agriculture is declining. Primarily in the western United States, water management has become a complex issue [3–6] which is further aggravated by a semi-arid climate, periodic drought and low precipitation [2,7,8]. A collective large-scale irrigation scheme is often established to manage the irrigation in such regions; hence, evaluating and improving the performance of the system is a critical step towards establishing better water management practices [9].

The proper evaluation of an existing system is also one of many ways to achieve several of the Sustainable Development Goals (SDGs) developed by the United Nations

(UN) in 2015. Goal no. 2 aims to “end hunger, achieve food security and improved nutrition, and promote sustainable agriculture”. Insufficient irrigation water is a major threat to food security in water-scarce areas; hence, the study of crop water consumptions and finding ways to ensure ‘more crop per drop’ are ways to attain this goal. Moreover, studies of this kind will also assist us in identifying the proportion of agricultural area under productive and sustainable agriculture, which is one of the indicators developed by the UN to track the progress for this goal. In addition to this, goal no. 6 aims to “ensure availability and sustainable management of water and sanitation for all”. At the moment, population growth, agricultural intensification and urbanization are beginning to overwhelm the available freshwater resources [10–14]. With irrigation water being the largest consumer of freshwater resources, saving even a fraction of this can significantly ease the strain on other sectors [15,16]. The integrated challenge of maintaining water and food security to achieve SDGs 2 and 6 in such a short period of time requires the extensive study of existing agricultural areas.

The concept of irrigation performance assessment has shifted during the last 25 years, from traditional irrigation efficiency measurements to performance indicators [17–19]. Several performance indicators have been introduced, based on adequacy [20–22], equity [20,22,23] reliability [24], productivity [20,25] and sustainability [26,27]. Indicators based on adequacy and equity are greater in number and have been employed in several studies [18]. Roerink et al. utilized the concept of relative evapotranspiration (RET) to investigate irrigation adequacy and water deficiency severity [23]. A similar concept was employed in other studies [2,28]. Likewise, coefficients of variation for actual evapotranspiration were used as an equity measure by numerous studies [2,17,29]. More recently, the attention to performance indicators based on productivity is also growing, primarily in regions where water is limited. Crop water productivity (CWP) provides information about how effectively water is being expended [30]. CWP, along with water use, has been used to assess water savings measures at different scales in the past, including the basin level [31–33] the irrigation scheme level [29,34–36] and the administrative division level [37].

Important aspects of irrigation performance indicators are the accurate estimation of the crop evapotranspiration (ET) and its spatial distribution. Recent improvements in remote sensing and satellite image products offer effective ways to estimate the spatial variation of ET [38,39]. Over the last few decades, a number of remote sensing techniques have been developed and used to estimate ET in large areas [40], including vegetation index (VI) methods and surface energy balance (SEB) methods. In a VI-based method, a relationship between the crop coefficient (k_c) and VI is developed, and the ET is calculated based on the Food and Agriculture Organization (FAO) approach. [41] utilized the normalized difference vegetation index (NDVI) to determine the k_c and crop ET, and they derived ET maps on a regional scale. With a slightly different approach, [42] employed additional parameters, including the crop cover fraction and the soil evaporation, to establish a relationship with the k_c of a wheat crop. Unlike energy balance methods, these methods avoid complex processes of parameter estimation. However, the relationship developed between VI and crop coefficients varies with the location. Hence, it may require the modification and validation of the relationship in new setting [31].

Commonly used SEB models include the Surface Energy Balance Algorithm for Land (SEBAL) [43], Mapping Evapotranspiration at High Resolution using Internalized Calibration (METRIC) [44], and the Simplified Surface Energy Balance Index (S-SEBI) [45]. SEB models estimate the actual crop ET (ET_a) as a residual of the surface energy budget and capture the impacts of poor water management on ET_a [31,44]. Singh et al. evaluated different SEB models over the Midwestern US in the calculation of instantaneous ET_a for irrigated maize crops [46]. The reported relative errors, when compared with flux tower measurements, were less than 10% for all of the models. A modification of the METRIC version, wet METRIC, was used conjunctively by [47] in the Midwest US to estimate the seasonal ET_a. An R^2 value of 0.91 was obtained when comparing the modelled ET with the

eddy covariance tower measured ET. Although the residual methods performed well, with promising accuracy [31], the complexity of the calibration, data entry and manipulations, and executions of these models requires a certain level of expertise. A recently introduced automated version of the METRIC algorithm in the EEFlux platform is a promising approach to obtain ETa maps without complex calculations. Costa et al. estimated the maize water consumption for different stages of maize growth development based on the EEFlux platform, with promising results [48]. Likewise, Venancio et al. [49] assessed soybean ET using EEFlux ETa, and the variation of the ETa in field was accurately estimated by the model. While the traditional version of the METRIC algorithm has been widely used and tested, the automated version of METRIC lacks extensive studies. Its applicability for regional water management is scarce and yet to be studied.

Yield mapping is another important aspect for the computation of an indicator based on productivity. Primarily, two different approaches, including crop growth models and empirical models, have been used in the past to estimate the crop yield using remote sensing [50,51]. The first method, though accurate, is limited by data availability [52]. The empirical method, on the other hand, can be utilized to assess the within-field variability in a simple and effective way [53]. Past studies showed that VI can explain up to 80% of the within-field yield variability [54,55]. The NDVI is one of the most widely used vegetation indices for the estimation of crop yield. Crop yield highly correlates with NDVI at specific growth stages [37]. Hence, some studies have directly utilized the production statistics from census data and successfully extrapolated it to the pixel level using NDVI as a medium [31,37]. A gap is often seen to utilize these two data sources conjunctively, because national statistics are often used only at the time of RS data interpretation [31,56]. The statistics on the district levels are collected in an organizational framework, are regularly available, and are widely accepted. Therefore, a simple disaggregating approach of published yield statistics to the pixel level, using remote sensing, can also help fill the gaps between two data sources. This may assist stakeholders to make use of the RS technique effectively.

Functioning as one of the country's largest irrigation projects, the Imperial Valley (IV) provides a significant contribution to the economy, as well as the nation's diet, health, and wellbeing [57]. Although the valley is highly dynamic and productive, the dry environment, water-intensive crops, and limited water supply render challenges in its water management. It is one of the major areas stressed by the Federal Government and State of California for water conservation [58]. Recently, a water transfer agreement was introduced that requires the transfer of about 10% of the IV's total Colorado river allotment to other Southern Californian regions. This new strain has further amplified the challenge water that managers are facing in the Valley. The prospects of the development of a new water supply are very limited in this scenario. However, the hospitable conditions of the Valley's environment support the growth of multiple crops, which would otherwise have been imported from other countries, adding a high economic value to its agriculture. Therefore, the proper assessment of the existing irrigation systems in the valley may help to identify the fields with low performance levels, where water management could be focused.

In this study, we quantified irrigation performance indicators based on adequacy, equity, and productivity, utilizing EEFlux ETa, NDVI and county-level statistics of the crop yield in the IV. The study focuses on fields where alfalfa and sugar beet crops are grown. A linear interpolation was performed in order to generate daily ETa maps for the crops' growing seasons in 2018 and 2019, which was further summated to obtain the total ET for the whole year. The computed ET was verified with literature-reported values and the ET computed from crop coefficient-reference evapotranspiration (kc-ETo) approach. Landsat NDVI images corresponding to the early growth stages for both crops were utilized to disaggregate the county-level yield statistics to the pixel level. A crop map was utilized to generate the crop specific ETa and yield map. We computed the seasonal RET as a ratio of the actual to the potential ET in order to assess the adequacy of the water in the fields. The United States Bureau of Reclamation (USBR) field boundary was utilized to estimate the coefficient of variation (CV) of the actual ET within and among fields, as a measure

of equity. A CWP map was produced as a ratio of the crop yield and ETa. High and low zones of the indicators were identified, and possible reasons, along with prospects for improvement and implications were devised. Additionally, a relationship of the CWP with the yield and ETa was also interpreted in order to identify the possible scope of the water management through CWP enhancement. Research questions of interest include: (1) What is the accuracy of EEFlux ETa compared to the literature-reported values and ET from kc-ETo approach? (2) How do high- and low-performance fields differ in proportion and location in the valley? (3) What is the scope of water conservation through water productivity enhancement for high water-use crops?

The remaining document is organized as follows. In the next section, the datasets used for the research are properly outlined, along with the sources and data characteristics. After this section, the research methods are explained progressively. Subsequently, the research results and findings are explained, followed by a discussion. The references are listed at the end.

2. Study Area

The study area for this research is the IV, within the extent of the Imperial Irrigation District (IID) (Figure 1). The IV covers an approximate area of 2.07B sq. m (512,163 acres). It consists of very productive soils, resulting from the periodic flooding of the Colorado River in the past. Because of the extremely hot and dry climate, scant rainfall, and water-intensive crops, the Valley requires an extensive amount of water for its agriculture to thrive. Approximately 3.8B m³/year (3.1M aft/year) of irrigation water is imported from the Colorado River, and its delivery to the field is managed by the IID. More than 4828 km (3000 miles) of canals and drains have been constructed for this purpose. The availability of irrigation water and rich soil makes it possible to grow hundreds of crops year-round amidst harsh climatic conditions. The major crops include alfalfa, sugar beet, sudan grass hay, winter vegetables, wheat and corn. Alfalfa supports huge industries of cattle and dairy production, and sugar beet is only produced in the IV among western US states. Both crops are grown year round, require intensive irrigation and have high field coverage. Hence, the study of the water use for alfalfa and sugar beets is the focus of this study.

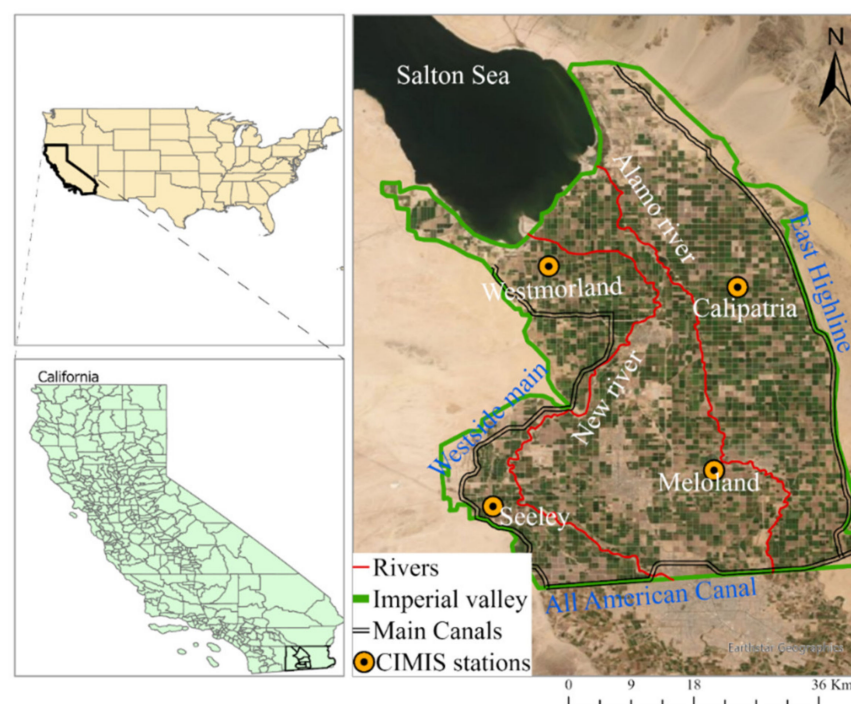


Figure 1. Study area location map that shows the major rivers flowing through the valley, as well as the major canals and meteorological stations.

Alfalfa is usually planted from mid-August to mid-March and is harvested three to four times a year. Sugar beets are planted between early August and October and are harvested between mid-April and mid-August. This study covers a full growing season of sugar beets from October 2018 to August 2019. Because alfalfa has a 3–4-year cropping cycle, the 2019 crop year was considered for the study. Hence, any crop-specific information and mapping presented in this study corresponds to each crop's growing season.

The weather conditions throughout the study period are shown in Figure 2. The weather data were obtained from the California Irrigation Management and Information System (CIMIS) (<https://cimis.water.ca.gov/>, accessed on 9 November 2020) for four stations located in the IV (Figure 1), and averaged. The average minimum (1.35 m/s) and maximum wind speeds (3.33 m/s) were observed during December and May, respectively. The mean solar radiation was high during most of the spring and summer months, and relatively low during the winter. Likewise, the average monthly temperatures were high most of the year, and ranged between 53 and 93 °F. The warmest month of the year was August (93 °F), whereas January and December (53 °F) were the coldest. The valley experienced the most rainfall during late summer and winter. Precipitation as high as 17.18 mm was observed on 25 September 2019, whereas June, July, August and October did not experience any rainfall in 2019.

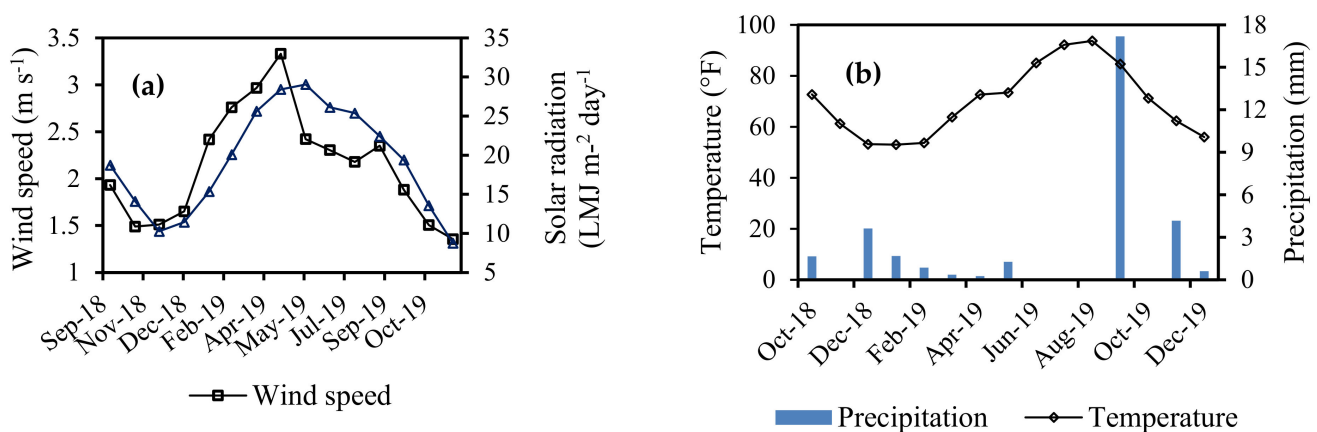


Figure 2. Weather conditions in the IV during the study period. (a) Monthly average windspeed and solar radiation, (b) monthly average temperature and precipitation. The value denotes the averages from four stations located in the valley.

3. Materials and Methods

The research approach to quantify the irrigation performance indicators based on adequacy, equity and productivity utilizing the EEFlex ET, NDVI and county-level statistics of the crop yield in the IV is presented in this section. Seven sub-sections are designated to explain the process. The Section 3.1 provides information on the key datasets. The image preprocessing steps are explained in the Section 3.2. The crop classification approach is explained in the Section 3.3. The description of the mapping of the seasonal ET is presented in the Section 3.4. The Section 3.5 explains the approach for the yield mapping, followed by the accuracy assessment and validation in the Section 3.6. The Section 3.7 explains the method used to compute the performance indicators. The estimation of each indicator is explained in a separate section.

3.1. Datasets

This section provides the description of the datasets used in the study. Each sub-section presented below summarizes the data types, the sources and their specifications.

3.1.1. Google EEFlux Datasets

The Landsat images for the ET calculation (Table 1) used in this study were processed on EEFlux/METRIC version 2.0.3 on the EEFlux website. EEFlux can be accessed freely at <https://EEFlux-level1.appspot.com/> (accessed on 10 November 2020). EEFlux utilizes the thermal and short-wave infrared band of Landsat to estimate the surface energy balance, vegetation amount, albedo and surface roughness. The ETa is computed as a residual of the surface energy balance [44], then calibrated mechanically using the gridded weather data. The ET is expressed in terms of ETrf, which represents the ET as a fraction of the reference ETr (alfalfa reference ET). Additional Details on the EEFlux METRIC processing are provided in Section 3.2. We processed a series of 25 Landsat scenes for the ETrf computation on the EEFlux platform. Both the Landsat 7-Enhanced Thematic Mapper (ETM) and the Landsat 8-Operational Land Imager (OLI), along with the Thermal Infrared Sensor (TIRS) scenes with cloud cover less than 10%, were collected to compensate for large data gaps during the interpolation. The images from December 2018 for both platforms were unusable due to high cloud cover, and hence were not considered. All of the Landsat 7 images obtained after 31 May 2003 had continuous data gaps due to the failure of the Scan Line Corrector (SLC). Therefore, the data gaps in the Landsat 7 scenes must be corrected by the user.

Table 1. Details of the Landsat images acquired in this study for processing in the EEFlux platform.

Satellite	Image Acquisition Dates			
Landsat-7 ETM	17 February 2019			
	8 May 2019			
	24 May 2019			
Landsat-8 OLI and TIRS	4 October 2018	29 March 2019	19 July 2019	23 October 2019
	5 November 2018	16 April 2019	4 August 2019	8 November 2019
	21 November 2018	30 April 2019	20 August 2019	24 November 2019
	24 January 2019	1 June 2019	5 September 2019	10 December 2019
	25 February 2019	17 June 2019	21 September 2019	
	13 March 2019	3 July 2019	7 October 2019	

3.1.2. Satellite Images for NDVI Mapping

Landsat-8 OLI and TIRS images for 13 March 2019 were obtained for the crop-specific NDVI computation. The images were downloaded from the United States Department of Geological Survey (USGS) website. Primarily, the Near Infrared (NIR) and red bands were utilized for the NDVI calculation. In this study, we utilized NDVI images to perform linear regression with the crop yield data for the yield mapping. Previous studies have shown that NDVI correlates well with the alfalfa yield during the second cutting and 10% bloom [59]. Similarly, a good correlation with the sugar beet biomass was observed during the crop development stage ($NDVI < 0.85$) before leaf senescence in a study by [1]. In semi-arid areas like California, the first alfalfa cutting period is approximately 60 days, and takes place during January and February [60]. After the first cutting, alfalfa is cut every 30 days, starting from March. Therefore, the image of 13 March belongs approximately to the early growth stage of alfalfa. For the sugar beets, we computed the average NDVI in the sugar beet fields during several months, starting from January. An average NDVI of 0.8 was observed for the 13 March image, and hence was considered for the NDVI mapping.

3.1.3. Reference Evapotranspiration

The reference ET was obtained from the CIMIS website. The CIMIS is a database maintained by the California Department of Water Resources (DWR). The ET dataset that CIMIS provides is a standardized ET based on the alfalfa (ETr) or grass surfaces (ETo) where each CIMIS station is located. The estimates of reference ET were carried out by CIMIS based on the CIMIS Penman's method. The CIMIS Penman method is the modified version of Penman equation created by [61]. The detailed steps used to compute the CIMIS

Penman's ET are described here: <https://cimis.water.ca.gov/Content/PDF/CIMIS%20Equation.pdf> (accessed on 5 May 2021).

In this study, we retrieved the daily ETr and ETo values over the study period (4 October 2018 to 10 December 2019) from four stations located in the IV. The EEFlux utilizes ETr during the calibration of the algorithm [49]. Because CIMIS has only one station based on the alfalfa's surface, the daily ETos from the remaining stations were converted to ETr by multiplying them by a factor of 1.23 [60] in order for the further processing to be consistent with EEFlux.

3.1.4. Data for the Crop Mapping and Validation

The mapping of the crop areas is required in order to quantify and map the crop-specific water consumption, yield and performance indicators. In this study, Sentinel-2 Level-2A images were acquired from the European Space Agency (ESA) (Paris, France) on the Sentinel Scientific Data Hub website for crop mapping. The satellites systematically acquire optical imagery including 13 spectral bands. The four visible bands have spatial resolutions of 10-m, the six infrared bands are at 20-m resolutions, and the remaining three bands are at 60-m resolutions. Level 2A products do not require atmospheric correction, as they are corrected for atmospheric effects before their delivery to users.

In addition, as a reference dataset to collect the training samples for crop-specific and non-crop categories, the Cropland Data Layer (CDL) products were acquired from the National Agricultural Statistics Service (NASS), United States Department of Agriculture (USDA) (Washington, U.S). The field-level crop data were obtained from Lower Colorado Water Accounting System (LCRAS), United States Bureau of Reclamation (USBR) (Washington, U.S), in order to assess the classification accuracy. The dataset contains the Geographical Information System (GIS) layer, which shows the crops grown throughout the year within the extent of the IID. The crop acreage estimates for each year were obtained from crop reports published by the IID's water department for the validation of the extracted area.

3.1.5. Other Datasets

No other spatially explicit ETa data were available to assess the accuracy of the ETa map prepared in this study. Hence, the ET reported in Table 1 of [58] were extracted for comparison with the EEFlux-computed Eta (Table 3). It includes the ET computed for the IV, as well as other western states for the two crops studied. Although the reported values represented point measurements, and were associated with methodological differences, the datasets were the best available reference to access the accuracy. In addition, the ETa was also compared with the ET computed using the kc-based procedure (ETc), in which the ETo is multiplied by kc to produce an estimate of the ETc. In order to do so, the kc values of alfalfa and sugar beet at different growth stages were obtained from various reference studies in the Western US and worldwide, as listed in Table 2. Crop-specific yield data for 2019 was obtained from Agriculture Commissioner reports. The shape files of the field boundaries were provided by USBR.

Table 2. Kc values from the literature used in this study.

Crop	Kc			Location	References
	Ini	Mid	Late		
Alfalfa	0.87	0.91	0.86	Argentina, semi-arid area	[62]
	0.6	1.1	1.1	California	[63]
	0.3	1	0.95	Idaho	[64]
	0.4	1.04	0.98	-	[60]
Sugar beet	0.2	1.17	1.12	California	[65]
	0.35	1.24	0.78	-	[60]

3.2. Image Preprocessing

The Google EEFlux platform was used to process the Landsat scenes for the ETrf calculations. EEFlux utilizes the METRIC algorithm, which computes the energy expended during the evapotranspiration process as a residual of the surface energy balance according to Equation (1):

$$LE = R_n - G - H \quad (1)$$

where LE is the latent heat flux or energy consumed by ET ($W m^{-2}$), R_n is the net radiation, G is the soil heat flux ($W m^{-2}$), and H is the sensible heat flux ($W m^{-2}$).

In order to extrapolate the LE for each pixel from the exact moment of the passage of the satellite to the instantaneous value, the LE is divided by the latent heat of vaporization using Equation (2):

$$ET_{inst} = 3600 \frac{LE}{\lambda \rho_w} \quad (2)$$

where ET_{inst} is the instantaneous ET ($mm h^{-1}$), λ is the latent heat of vaporization ($J kg^{-1}$), and ρ_w is the density of water.

The resulting ET_{inst} is expressed as ETrf, which represents the fraction of the reference evapotranspiration (ETr) (Equation (3)). ETr is the reference evapotranspiration based on alfalfa, as defined by the ASCE Standardized Penman-Monteith equation [66]. EEFlux computes ETr using gridded hourly and daily weather data stored in the Earth Engine.

$$ETrf = \frac{ET_{inst}}{ETr} \quad (3)$$

ETrf can be used to estimate the actual ET for any period by multiplying it with the ETr for nearby stations. In the EEFlux platform, the image size that can currently be downloaded is limited and does not cover the entire study area. Hence, the resulting ETrf maps were mosaicked for each image date in ArcGIS Pro. In addition, the data gaps in the images from the Landsat-7 platform were filled using the nibble tool in ArcGIS Pro. The nibble tool replaces the cells of the raster with the values from the nearest neighbors.

3.3. Crop Classification

We classified a Level-2A S2 image of 6 April 2019 using a machine learning approach, i.e., a random forest (RF) algorithm. The image corresponds to the pre-harvest period for most of the crops in the field. Before classification, the 10 bands of S2 (aerosol bands not included) were resampled to 10-m resolutions using a bilinear resampling method. Five crop classes grown in the Valley were considered, including alfalfa, mixed grasses, wheat, corn, mixed crops and sugar beets. Mixed grasses include hays, excluding alfalfa (turf grass, bermuda grass, klein grass, etc.). All of the vegetables and remaining crops were included in the class of mixed crops. The non-crop classes included built-up, water bodies, and fallow. Though the non-crop classes were included during the classification process, the results were only interpreted in terms of the alfalfa and sugar beets, the main focus of this study. The CDL layer from the USDA was used as the reference dataset to collect the training samples for crop-specific and non-crop categories. Polygons, representing various crop types, were sampled from the Sentinel image, in which the identification of the crop type was performed based on a cropland map. We utilized the 'randomForest' function in the 'randomForest' package of R version 4.0.2 for the crop classification. Independent reflectance values from each band of S2, along with NDVI, were used as features during the crop categorization. A confusion matrix was prepared between the ground truth datasets provided by the USBR and Sentinel-identified crop types in order to evaluate the classification accuracy. The predicted crop acreages were validated with acreage statistics provided by the IID. The crop map was resampled to a 30-m resolution after accessing accuracy to use with 30-m resolution Landsat-derived products. Then, alfalfa and sugar beet polygons were extracted from the resampled classified map, and two distinct crop layers representing the crops were prepared to be used for further analysis.

3.4. Mapping the Seasonal ET

The series of ETrf maps of the study area, obtained from the EEFlux platform, were used as a vehicle to extrapolate the ETa for the whole season. At the beginning, daily ETrf maps were generated for each day between the image dates by means of linear interpolation. The interpolation was performed in R statistical software version 4.2. The `Approx()` function in the base R package was utilized. Two sets of computations were performed in order to obtain daily ETrf maps, with each corresponding to the growing seasons of the crops studied. We interpolated images from 24 January 2019 to 10 December 2019, which were utilized later for the ETa computation of alfalfa, whereas images from 4 October 2018 to 20 August 2019 were interpolated in order to compute the ETa for sugar beets. The daily ETrf images obtained after interpolation were multiplied by the ETr of each day, then totaled to obtain the cumulative ET for the whole season (Equation (4)). The ETrs from four weather stations were averaged for each day.

$$ET_{\text{period}} = \sum_{i=m}^n [(ETrf_i) \times (ETr_{24i})] \quad (\text{Allen et al., 2007}) \quad (4)$$

where ET_{period} is the cumulative ET starting from day m to n , $ETrf_i$ is the interpolated ETrf for day i , and ETr_{24i} is the 24 h ETr for day i .

An overlay of the seasonal ET map with the classified crop map of the study area was made in order to obtain a seasonal ET map for individual crop classes.

3.5. NDVI and Yield Mapping

The Landsat images utilized to compute the NDVI for 13 March 2019 were atmospherically corrected before further processing. The Digital Number (DN) was converted to the at-surface reflectance using the formula provided by the USGS. The required information, including the multiplicative rescaling factor, additive rescaling factor and local sun elevation angle, were obtained from the metadata files. Then, the NDVI was computed using NIR and red band.

In order to obtain the crop yield map at the pixel level, the yield information of the crops obtained from the crop report was disaggregated using the Landsat NDVI data as a bridge [31]. An assumption was made that the NDVI of the crops during the growing season is directly related to the yield. The higher the NDVI of the crops, the higher the yield would be. Hence, a weighting factor (WF) was defined as the ratio of the pixel-wise NDVI for the crop of interest to the average NDVI for the Valley (Equation (5)). WF was related to the observed yield statistics using Equation (6). The equation generated a crop yield map with a resolution of 30 m.

$$WF = \frac{NDVI_{\text{pixel}}}{NDVI_{\text{avg}}} \quad (5)$$

$$Yield_{\text{pixel}} = WF \times Yield_{\text{obs}} \times \text{Area of one pixel} \quad (6)$$

where $NDVI_{\text{pixel}}$ and $NDVI_{\text{avg}}$ are the NDVI of an individual pixel and the average NDVI for the crop of interest, respectively. A crop-specific map of $NDVI_{\text{pixel}}$ was masked out utilizing the crop map. $Yield_{\text{obs}}$ is the observed yield from the report, and $Yield_{\text{pixel}}$ is the yield of any given pixel for the crop of interest in kg/m^2 .

3.6. Validation of ETa and Yield

The Mean Absolute Deviation (MAD) and Relative Error (RE) were computed in order to assess the associated differences between the computed ETa and the values reported in the literature for the IV. In addition, we computed the ETc for each crop using the kc values from the other reference studies, as well as those from [60], and compared this with the EEFlux ETa. The grass reference ETs (ETo) from three CIMIS stations were obtained for days corresponding to initial, mid- and late growth stage of the crops, then multiplied with

the k_c from Table 2 to obtain the ET_c values. The FAO-56 specified k_c values represented the standard climate, with the mean daily minimum relative humidity (RH_{min}) equal to 45% and the mean daily wind speed (WS) equal to 2 ms^{-1} . When the mean weather differs from the standard, k_{cmid} and k_{clate} has to be adjusted as described in Allen et al. (1998) [67]. This procedure was followed in this study, and Table 2 represents the adjusted values. The mean ET_a from EEFlux were extracted for similar days. The Root Mean Square Error (RMSE) and Mean Absolute Error (MAE) were computed between the two, and the results were analyzed. The pixel-wise yield assessment was also restricted due to limited data. Therefore, for validation, the pixel-wise yield values were summed and compared with the reported total crop production. Because the model is the linear extrapolation of the field data reported by the county itself, the quality of the yield map produced can be considered acceptable.

3.7. Computation of the Performance Indicators

Several performance indicators are available to evaluate the existing practices in the field and identify room for efficient water management improvement. Hence, the selection of the appropriate indicators is needed, which should be based on the purpose of the assessment and the availability of data [68]. Surface energy balance models are direct indicators of equity and adequacy [18]. Productivity indicators based on yield and ET_a can provide valuable insights for the identification of the scope of water management, where water is the limiting factor [34]. Therefore, considering the aforementioned factors, three indicators were chosen in this study, and their computation methods are explained in several subsections below.

3.7.1. Water Consumption Uniformity (WCU)

WCU is the indicator of the irrigation equity or the uniformity of water consumption [18]. Measurements of equity based on water consumption, rather than on the supply side, are considered more relevant in water-scarce regions [17]. The WCU was evaluated by computing the CV of the ET_a at two levels in this study. The availability of field boundaries from the USBR allowed for the calculation of the CV within the fields (CV_w). The zonal statistics tool in ArcGIS Pro 2.5 (ESRI, 2020) was utilized for this purpose. The crop map prepared in this study contained several scattered pixels, which might have resulted from misclassification. Therefore, in order to avoid the inclusion of such pixels during the CV_w computation, the fields with less than 40 pixels ($\sim 36,000 \text{ m}^2$) were masked out from the crop-specific ET_a map beforehand. The threshold was set after visually analyzing the crop map prepared. Hence, the mean and standard deviation of the ET_a were obtained for fields with areas larger than $36,000 \text{ m}^2$. The number of alfalfa fields studied was reduced from 4183 to 2481, and the number of sugar beet fields from 817 to 478 after masking out the redundant pixels. In addition to CV_w, we also computed the CV of ET_a among the fields (C_{va}).

3.7.2. Relative Evapotranspiration (RET)

RET is the indicator of the water adequacy in the field, and it provides essential information on crop stress and water shortages. In the present study, RET is computed as the ratio of seasonal ET_a to ET_p . ET_p refers to the maximum crop evapotranspiration under the optimal crop growing conditions, with no limitation based on plant growth. It is similar to the theoretically computed ET. Therefore, ET_p was expressed as a product of seasonal ET_o and k_c [31]. The daily ET_o measurements from the CIMIS stations were summed to obtain the seasonal value at each station. Then, the station location information was utilized, and seasonal ET_p raster maps were generated from the point measurements using Inverse Distance Weighting (IDW) interpolation. The algorithm was implemented in ArcGIS Pro. A seasonal k_c value of 0.9 was used for alfalfa [7,60]. The seasonal k_c for sugar beets was computed using k_c values from [60]. The weighted average of k_c computed according to the growing season length resulted in a seasonal k_c of 0.9 for sugar beets.

3.7.3. CWP

The CWP was estimated for the study area using the crop specific ETa and yield maps from Equation (7). Any differences in units from the yield map and ETa were adjusted to calculate the CWP in kg/m³.

$$\text{CWP (kg/m}^3\text{)} = \frac{\text{Crop yield (ton/acre)}}{\text{ETa (mm)}} \quad (7)$$

In order to identify the field or areas with significant scope of improvement, the CV of the CWP in the study area was computed. A low CV of CWP indicates homogeneity and limited scope for improvement, whereas a high CV for an area indicates the opportunity of water management [34]. The relationships of CWP with ETa and yield were also looked at in order to evaluate the scope of CWP enhancement in the field under the current cropping conditions.

4. Results

The results and discussion are organized into five sections. Section 4.1, the results of the crop classification are presented. The spatial distribution of ETa and yield are presented and discussed in Section 4.2. The accuracy assessment of the computed ET is discussed in Section 4.3. Following this section, the outputs from the performance indicators are explained in Section 4.4. Section 4.5 primarily discusses the scope of the water management improvements in the Valley, as depicted by the performance indicator results.

4.1. Crop Classification

The overall accuracy of the crop mapping obtained was 85%. The individual assessment of the crop prediction accuracy showed that sugar beets were the most accurately mapped, with a producer accuracy of 99.5%. Alfalfa was also mapped reasonably well, given its wide distribution in the field. The accuracy of alfalfa was 85.2%. Several mixed grasses and mixed crops in the field were incorrectly labeled as alfalfa, which resulted in an alfalfa prediction commission error. The researchers mostly identified the confusion between alfalfa and mixed grasses. A similarity in the spectral signatures between alfalfa and mixed grasses could be the reason for it. The comparisons between the predicted and observed crop acreages showed that, for S2, there was underestimation of the alfalfa crop area by 16.65%, and of the sugar beets by 4.38%. The slightly high difference in the alfalfa acreage could be attributed to the predominant presence of alfalfa in the field. Hence, the accuracies obtained for alfalfa and sugar beets were considered reasonable for further study.

4.2. Spatial Distribution of ET and Yield

Figure 3 shows the spatial distribution of the seasonal ETa for both crops in the Valley. Alfalfa showed a large spatial variation, with a CV of 23.86%. The mean ETa for alfalfa was observed to be 1388.26 mm. Though alfalfa's ETa ranged from 39.09 mm to 2064.93 mm (Figure 3a), less than 7.2% of the pixels were in the range of 39.09 mm to 849.43 mm. A small proportion of the alfalfa field clustered on the north corner exhibited a low ETa (849.43 mm–1659.77 mm). About 45% of the alfalfa fields had an ETa in the range of 1254.60 mm to 1659.77 mm, and this was scattered around the valley. However, fields with a high ETa, up to 2064.93 mm, were found to be visibly clustered largely on the eastern corner of the Valley. The high spatial variation for alfalfa may be attributed to the periodic cutting of alfalfa during the growing season. Similar to the alfalfa, the proportion of sugar beets with a low ETa, ranging from 124.87 mm to 763.25 mm (Figure 3b), occupied less than 8.5%. For sugar beets, the mean ETa was observed to be 1126.95 mm, and the CV was 21.36%. Approximately 78% of the sugar beet fields exhibited ETas from 763.25 mm to 1401.64 mm, clustered around northeast corner of the Valley. Less than 13% had high ETas, up to 1720.83 mm.

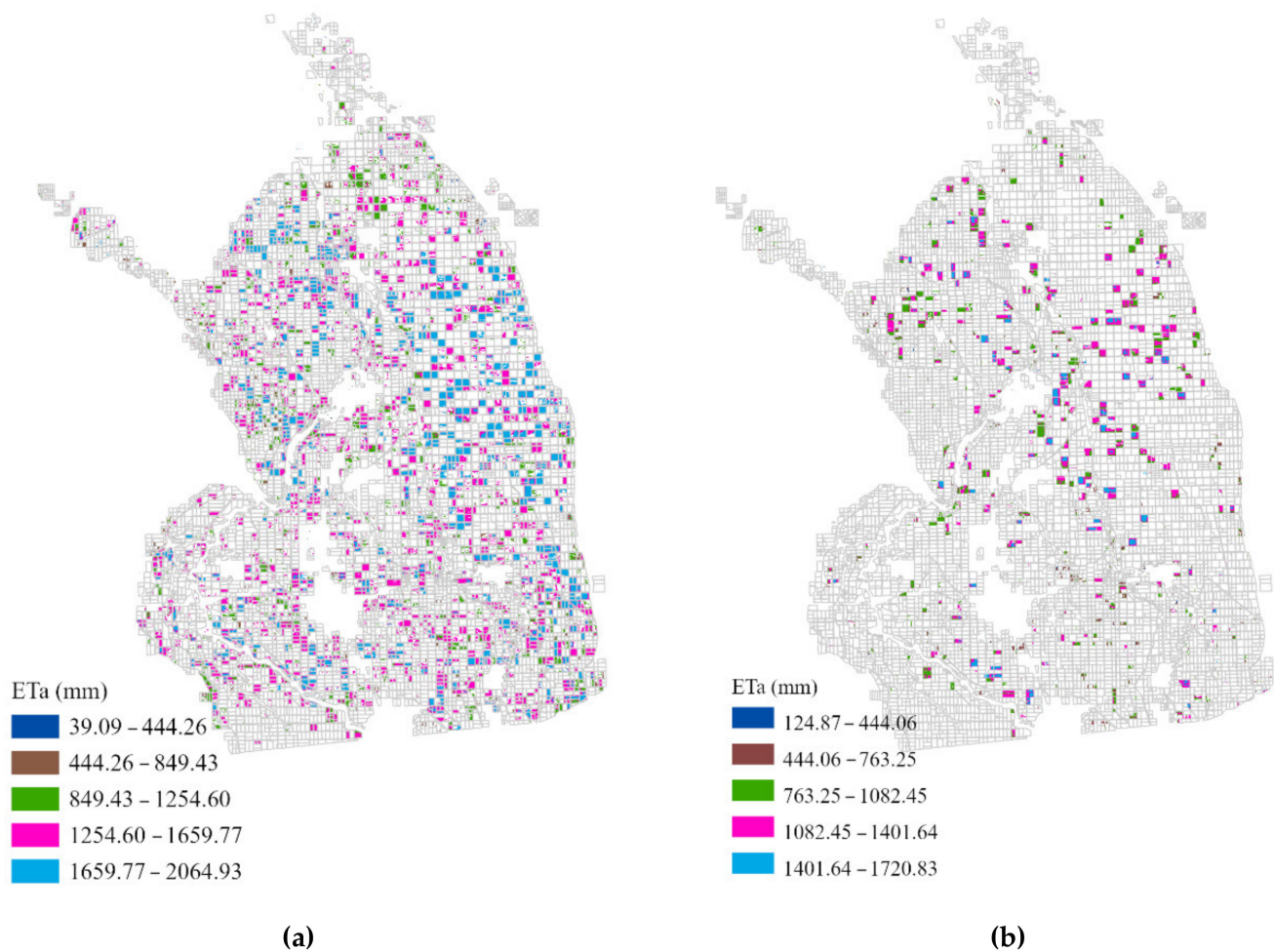


Figure 3. Spatial distribution of the growing season ETa for (a) alfalfa and (b) sugar beet. The ETa maps are overlaid with the USBR field boundary.

The alfalfa and sugar beet productivity maps resulting from disaggregation are shown in Figure 4. The average alfalfa yield for the study period was observed to be 0.395 kg/m^2 . Less than 2% of the areas exhibited yields in the range of $0.004\text{--}0.198 \text{ kg/m}^2$; hence, they are not visible in the spatial map presented (Figure 4a). The estimated range of the alfalfa yield in this study was close to the range predicted by [59] in Saudi Arabia, which was $0.179\text{--}0.628 \text{ kg/m}^2$. A few regions with visibly low yields (the brown patch in Figure 4a) were observed in the northern corner of the Valley. It should be noted that the ETa was also low in this area (Figure 3a). Besides this, it has also been identified that areas without a significantly high ETa (pink patch in Figure 3a) also exhibited high yields for alfalfa. In regard to sugar beets, the average yield was 2.351 kg/m^2 . Though 88% of the areas exhibited yields greater than 2.5 kg/m^2 , noticeable spatial variation among the fields can be seen after this range (Figure 4b). Regions with low yields were clustered at the northeast of the Valley (green patch in Figure 4b). Continuous fields of high yield were perceived in the northwest of the Valley, near the Salton Sea.

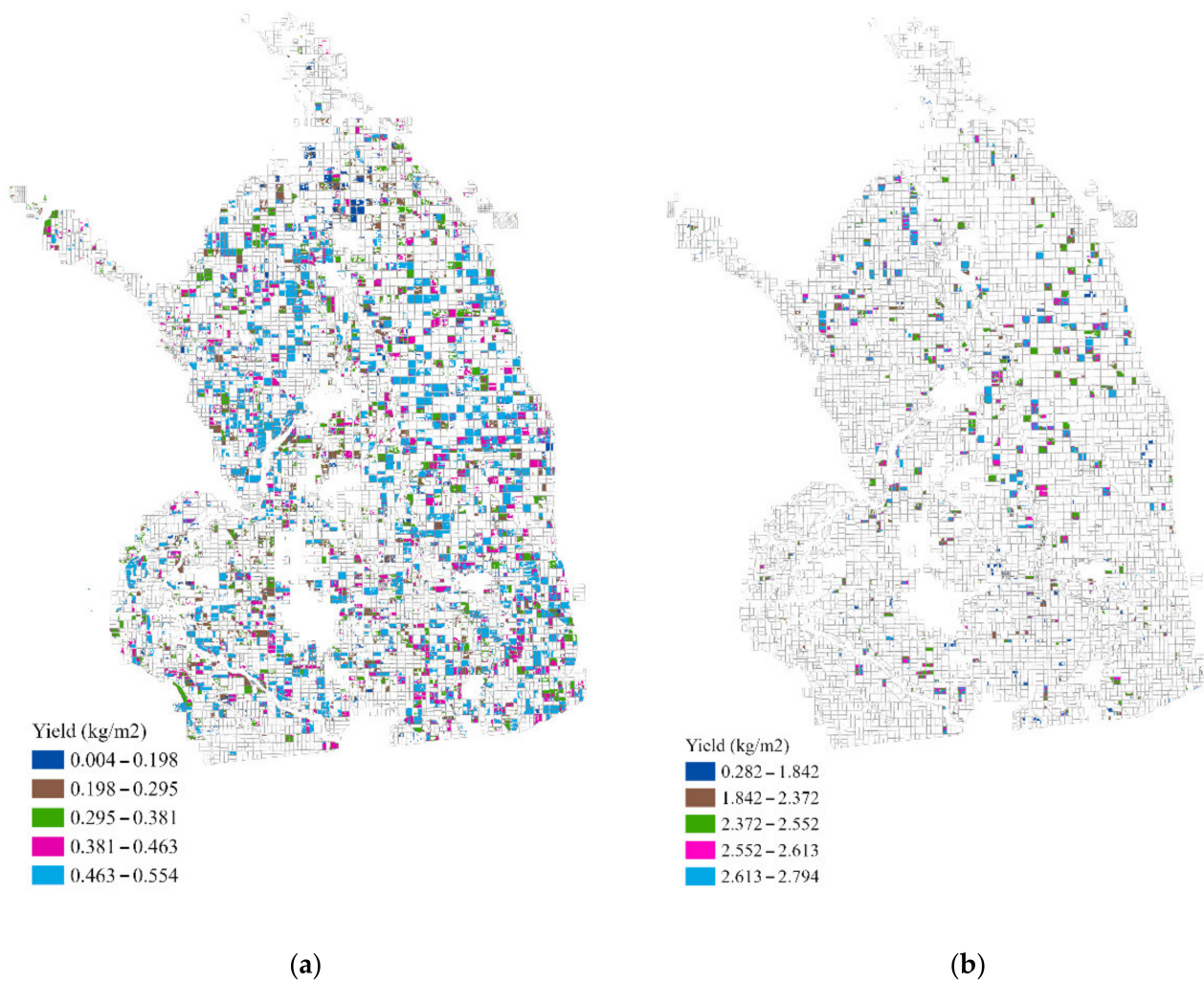


Figure 4. Pixel-based distribution of the growing season yields for (a) alfalfa and (b) sugar beet, in kg/m².

In order to analyze the extent of the differences between the observed and disaggregated production values, the distributed yield was aggregated. The absolute differences with the observed production were 13.55% and 2.9%, respectively. The resulting differences were because of the underestimation of the planted area during the crop classification. The pixel-level validity was limited due to a lack of ground truth data. However, because the modelled yield is based on the linear extrapolation of district data, it mostly relies on the input data consistency [31], which is officially accepted in the current study.

4.3. ET Validation

Section 4.3.1 describes the results of the validation of the computed Eta with the literature reported values. Additionally, the results of the comparison with the ET from the kc-ETo approach are explained in Section 4.3.2.

4.3.1. Comparison with the ET from the Literature

The alfalfa ET values obtained from the literature were mostly point measurements ranging from 1295.4 mm to 1889.8 mm. Table 3 shows the comparison between the predicted and observed ET from the literature. The MAD and RE of the alfalfa ETa were found to be as low as 46.43 mm/year and 7%, respectively, with the USDA. The computed values also showed reasonable agreement with [7], with an MAD of 134.37 mm/year and an RE of 16%. With the IID and USBR, the deviation ranged from 220.27 mm to 250.77 mm, and the RE ranged from 24% to 27%, respectively. For sugar beets, a very good

ETa agreement was obtained when compared with the point representative methods. The MAD and RE were found to be nearly null with the IID.

Table 3. Comparison of the EEFlux-derived ETa with ET values reported in the literature. The ET values for columns three to five were extracted from Table 1 of [58]. IID*, Imperial Irrigation District; USBR*, United States Bureau of Reclamation; USDA*, United States Department of Agriculture.

Crops	EEFlux Eta (mm)	ET (mm) from Literatures			
		IID*	USBR*	USDA*	[7]
Alfalfa	Mean = 1388.26 SD = 331.34 Max = 2064.9	1828.8	1889.8	1295.4	1657
		MAD RE	220.27 0.24	250.77 0.27	46.43 0.07
Sugar beet	Mean = 1126.95 SD = 240.82 Max = 1720.83	1127	1097.3	660.4	N/A
		MAD RE	0.02 0.00	14.83 0.03	233.28 0.71

Similarly, with the USBR values, an MAD of 14.83 mm/year and an RE of 3% was attained. Slightly high differences were observed with the USDA-measured values. The USDA-derived values were based on the Salt River Valley and Arizona; hence, climatological differences with the IV may have resulted in greater variances. The literature shows that the ETa computed from remote sensing can vary, with ground measurements in the range of 1 to 20% [69]. With METRIC, an RE of up to 13.7% was observed by [46], and up to 16% in the study by [70]. This shows that the difference exhibited in this study is within the plausible range. It should be noted that the values identified in the literature are not only associated with the methodological differences, scale of measurements, weather conditions, and year when the measurements were taken but also varied, which results in a complexity of comparison. Based on this fact, a relatively good agreement of the ETa with the point measurements provides strong evidence that EEFlux may be a valuable tool for the mapping of seasonal ETa.

4.3.2. Comparison with the FAO-56-Computed ETc

Figure 5 presents the mean ETa values during the initial, mid- and late season stages obtained from the present work, along with the ETc computed using the kc values from other reference works around California and other western states. The initial, mid- and late growth stages for alfalfa correspond to 1, 13 and 29 March 2019, respectively. Likewise, for sugar beets, they correspond to 5 November 2018, 1 February 2019, and 12 August 2019 for the respective growth stages. The values of the ET obtained from EEFlux for alfalfa have an initial phase value of 3.58 mm, an intermediate phase value of 3.25 mm and a final phase of 3.91 mm. Similarly, the values of 2.14 mm, 2.41 mm and 4.32 mm were obtained for sugar beets for the corresponding growth phases.

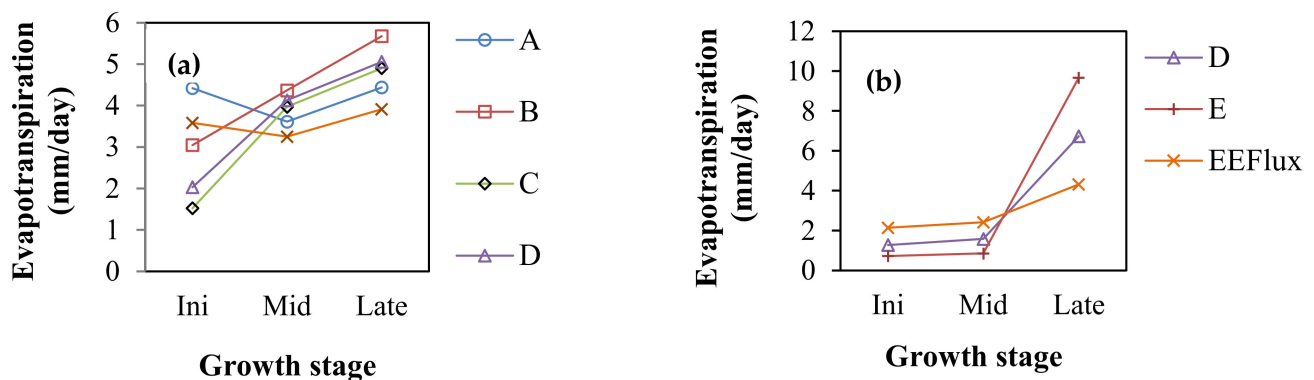


Figure 5. Comparison of the ET calculated from EEFlux METRIC with the ET computed using the kc-ETo approach for (a) alfalfa and (b) sugar beet. The kc values were obtained from A: [62]; B: [63]; C: [64]; D: [60] and E: [65].

It was observed that ETa showed a wide variation with the observed data. The RMSE and MAE variations for alfalfa from those in the literature ranged from 0.6 to 1.3 mm/day and 0.5 to 1.25 mm/day, respectively. When compared with the computed ETc using kc values from [60], the resulting RMSE was 1.22 mm/day, and the MAE was 1.19 mm/day. The ETa was overestimated during the initial growth stage, whereas it was underestimated in later stages. The sugar beet ETas computed in this study were like those obtained from the literature during the initial and mid-growth stages. The resulting RMSE and MAE were 1.5–3.3 mm/day and 1.3–2.7 mm/day, respectively, with the lower value range computed with the kc from [60]. The overall results suggest that EEFlux tends to underestimate the ETa during the mid and late stages of alfalfa growth, as well as the late growth stage for sugar beets. A similar result was obtained in the study by [48] for maize crops, and by [49] for soybean crops, using the EEFlux tool. In addition, [71,72] also reported low accuracy for cotton and coffee crops, respectively, using the SEBAL algorithm.

The low level of accuracy in general for EB algorithms, when compared to the computation based on the kc from [60] can be attributed to several reasons. First, EB algorithms consider the spatial variability of ET and kc, unlike other methods. Differences in the ET values may also be attributed to the variability of kc according to local growing conditions and land use management, as well as the rainfall and atmospheric conditions, including the air temperature, wind speed and vapor deficit [73]. In addition, FAO- kc values are derived from multi-day data (average values), while EEFlux METRIC obtains its kc, i.e., ET_{rf} values, at the satellite's passing time [48,49]. Because the evaporation from soil is usually higher immediately after rain or irrigation events, higher overall ET concentrations can be anticipated during this time [62]. The average kc values from the literature therefore consider both higher and lower evaporation rates from wet soil surfaces, whereas EEFlux ET_{rf} represents the actual conditions of the satellite overpass time [48].

4.4. Performance Indicators

In this study, three performance indicators based on equity, adequacy and productivity were studied for alfalfa and sugar beet fields. The results for each are explained in the separate subsections below.

4.4.1. WCU

ETa maps and field boundaries were used to calculate the coefficient of variation of the water consumption, also known as WCU, for the alfalfa and sugar beet fields. A problem associated with irrigation uniformity is suggested by the high variation of the water use within the fields [74]. Figure 6 shows the spatial variation of the CV_w for both crops. The CV_w for alfalfa ranged from 0.5% to 36.1% (Figure 6a), with the average being 9.7%. Although the map shows a CV_w as high as 36.1%, only 0.8% of the regions had variations greater than 21%. Hence, this may have resulted from the inclusion of some

partial crop coverage fields (Santos et al., 2008). Similarly, for sugar beets, the CVw of the seasonal ETa ranged from 0.2% to 22.2% (Figure 6b), with an average of 3.2%. Less than 0.23% of the regions had CVws greater than 18%. This could be explained by the same reason attributed to alfalfa. We also computed the field variability of the water use for both crops. A high variation of water use among the fields may indicate differences in farmers' irrigation practices [74]. The resulting variations were 19.36% and 19.9% for the alfalfa and sugar beet fields, respectively.

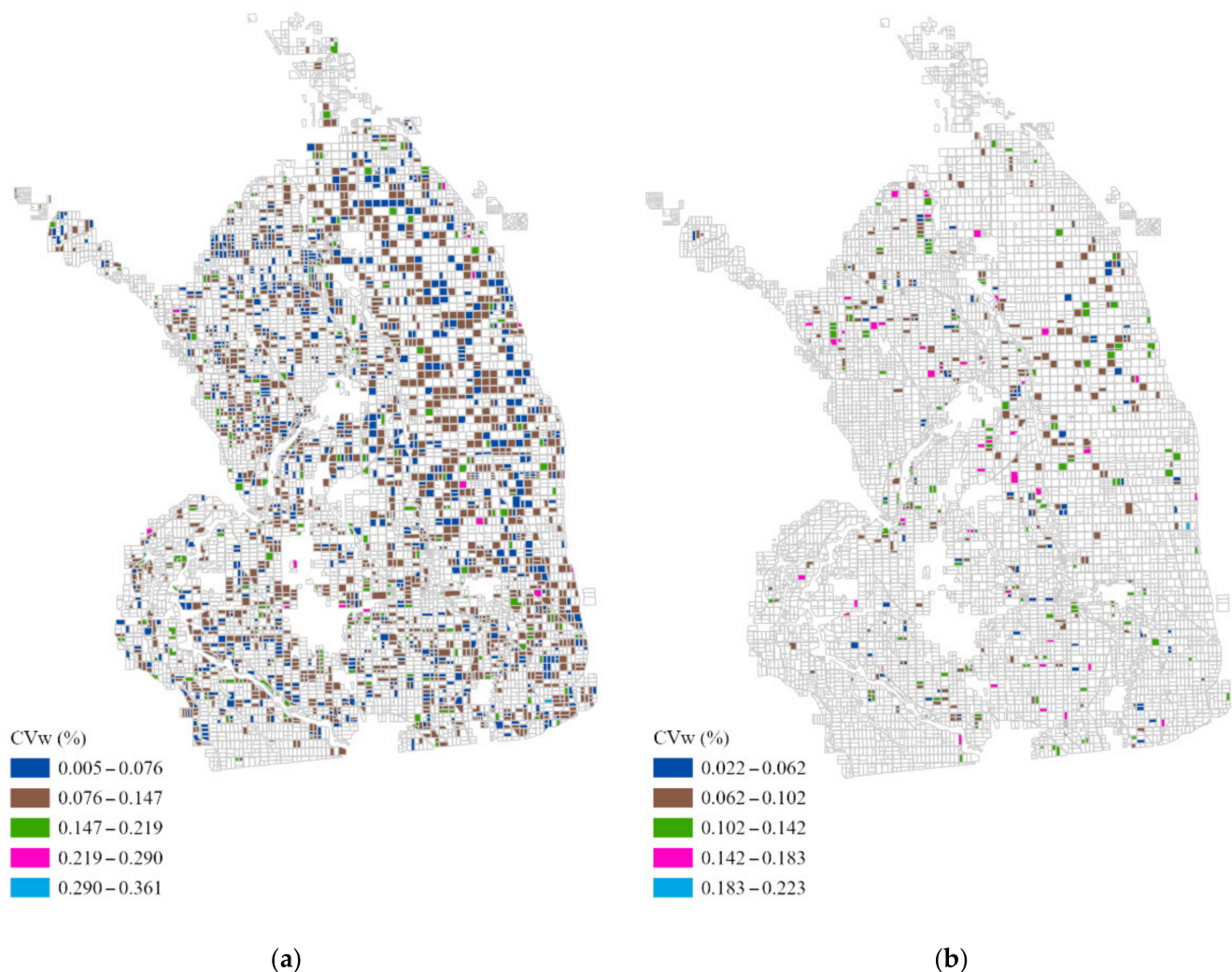


Figure 6. Within-field coefficient of variation for (a) alfalfa and (b) sugar beet fields, expressed in percentages.

Molden and Gates suggests a CV less than 10% to be good uniformity [75]. Approximately 36.14% of the sugar beets and 34.17% of the alfalfa exhibited CVws greater than 10% in our study. The focus on water management could be placed on those flagged fields, rather than the whole district. The overall greater uniformity in the Valley can be attributed to the application of various tilling methods, such as levelling and sod busting systems [76] for precise field grading. Similarly, greater Cvas for both crop fields suggest that the irrigation equity is slightly poor among the fields. The high Cva among the alfalfa fields could also be attributed to their continuous planting and harvesting. Overall, even though the average performance was satisfactory, the large variation in performance among farmers suggests that there is significant room for improvement.

4.4.2. RET

The ratio of the actual to the theoretical ET was used to calculate the adequacy for both crops, which is also called the RET. The spatial distribution of the RET is presented in Figure 7. The average RETs for the alfalfa and sugar beet fields were 0.844 and 0.797, respectively. The difference between ET_a and ET_p should be less under ideal growth conditions, and the ratio should be nearly equal to 1. Roerink et al. suggests that, for irrigated agriculture, values of 0.75 and higher are satisfactory [23]. In the current study, more than half of the planted area for both crops exhibited RETs greater than 0.75, suggesting satisfactory adequacy. Focus could be placed on the fields with RETs lower than the optimal value, where crops are experiencing water shortages that could result in poorly developed crops, affecting the yield [69].

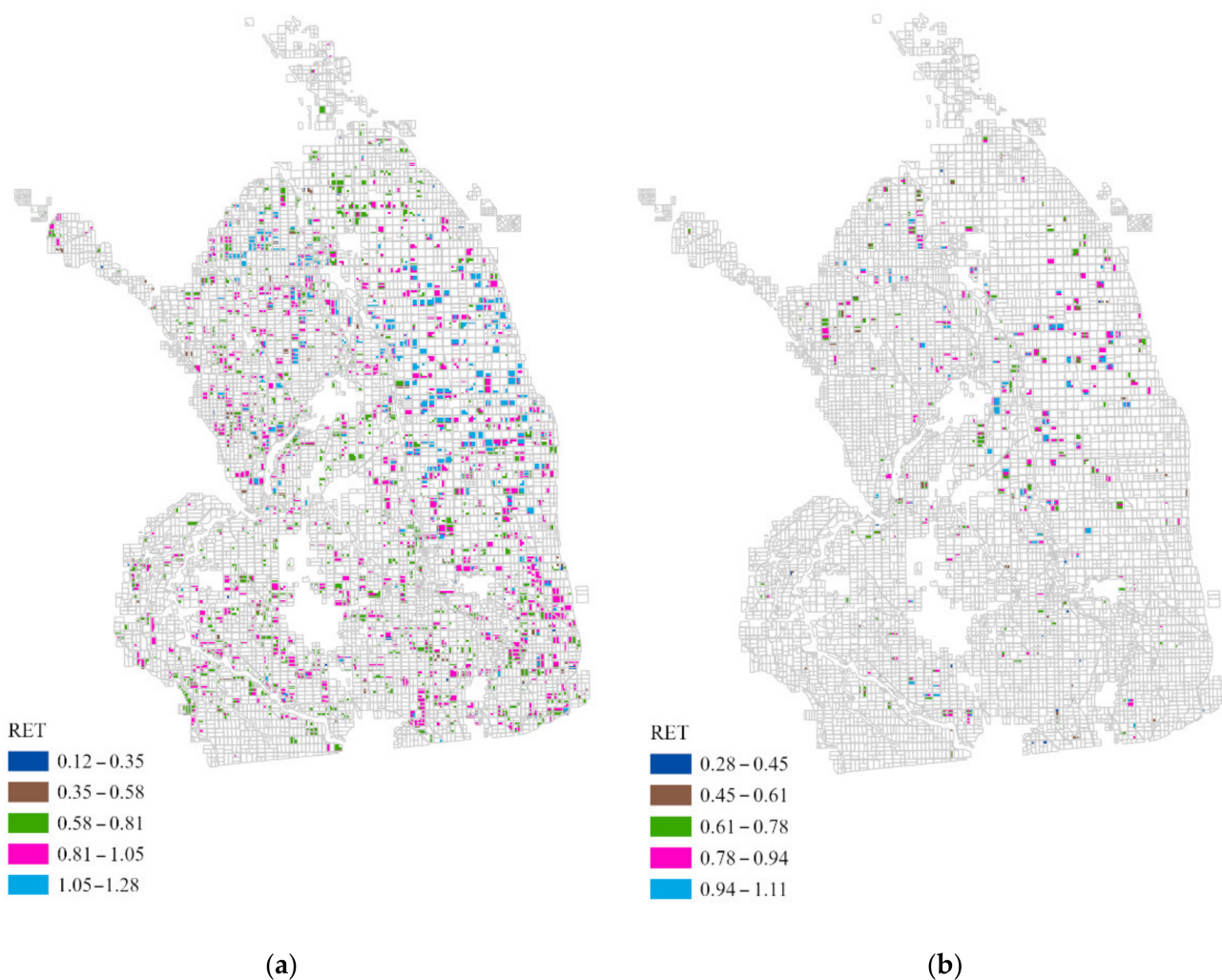


Figure 7. Spatial distribution of RET for (a) Alfalfa (b) Sugar beet fields.

The RET maps not only allowed us to identify the fields experiencing water shortages but also the fields consuming more water than their potential. About 31.5% of the alfalfa and 12% of the sugar beet fields had RETs of more than one. For alfalfa, these fields are visibly clustered on the east side of the valley (Figure 7a), whereas for sugar beets, fields in eastern regions and a few in the central regions exhibited RETs greater than one (Figure 7b). A slightly high average RET (0.97) was found for the Palo Verde Irrigation District (PVID), which is also located in Imperial County, in the study by [2]. The average was computed for the whole irrigation district, rather than the crop-specific fields, and using the Priestley–Taylor approach, which may have resulted in the differences. Bastiaanssen et al. [77]

reported a comparable average RET value of 0.77 in the Nilo Coelho irrigation system in Brazil, and 0.7 in the Gediz Basin in Turkey in a study by [28].

4.4.3. CWP

The water productivity was computed as a ratio of the crop yield to ETa in this study. Figure 8 shows the spatial map of the CWP for both crops. The average alfalfa CWP for the Valley is 0.328 kg/m^3 , with a CV of 32.92%. Although the alfalfa CWP ranged from 0.004 to 4.062 kg/m^3 , approximately 99% of the fields had CWPs of less than 0.8 kg/m^3 . The remaining fields were likely to be associated with mixed pixels with other crop types during the classification. The sugar beet CWP resulted in an average of 2.387 kg/m^3 , with a slightly lower CV (25.4%) than alfalfa. Like alfalfa, though the CWP exhibited a higher range for sugar beets, about 99% of the fields with CWPs of less than 4.6 kg/m^3 were observed, with the attributed reason being similar to that of the alfalfa. The average CWP of alfalfa obtained in the study was close to the range, $0.38\text{--}0.43 \text{ kg/m}^3$, recommended by [78] for Saudi Arabia; however, it was slightly lower than that reported in [79], which was 0.55 kg/m^3 . The variation in the climate and alfalfa productivity may have caused the differences.

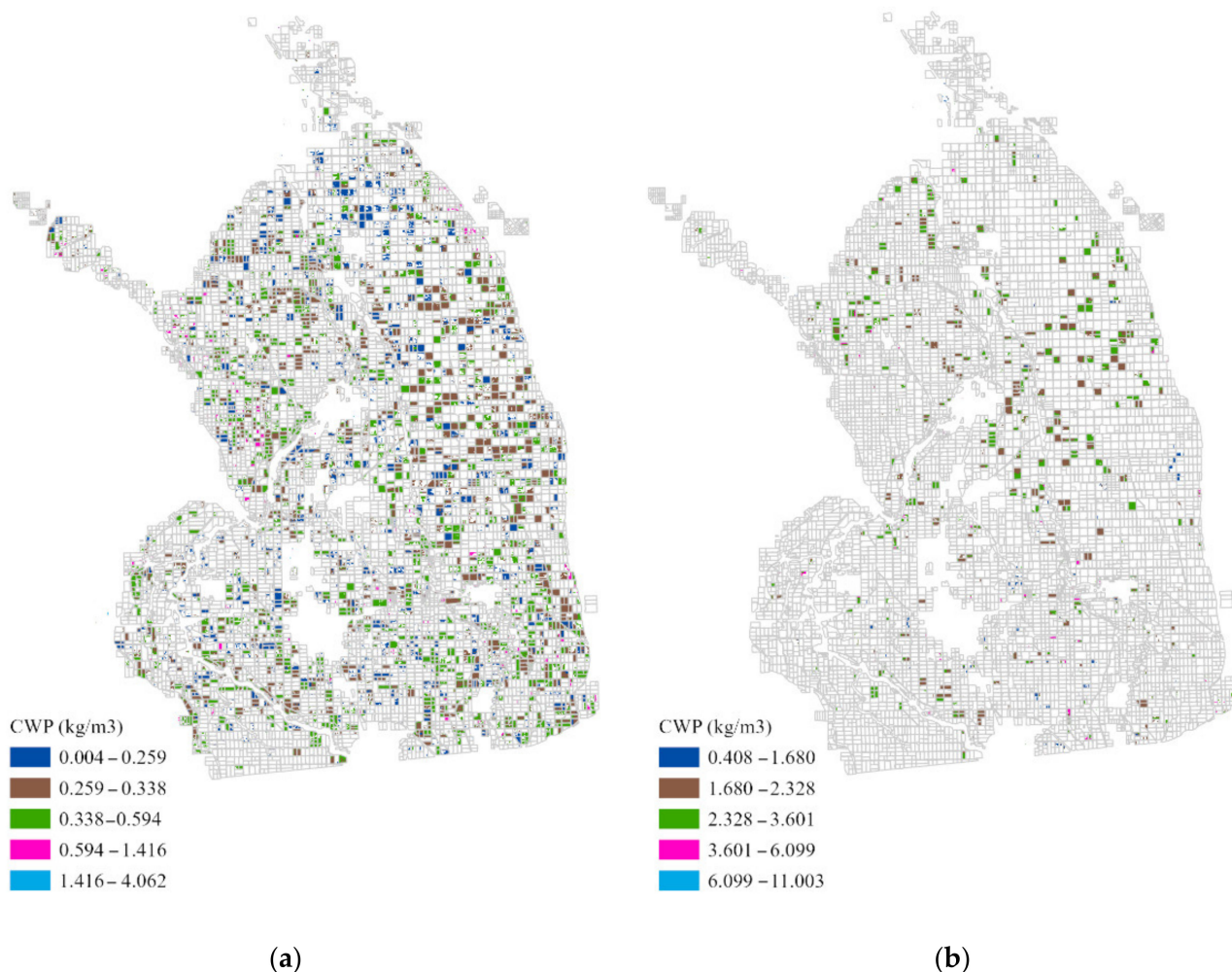


Figure 8. Spatial distribution of CWP for (a) alfalfa and (b) sugar beet fields.

The crop fields showed a mixed trend of CWP with ETa and yield. The northwest corner of the sugar beet fields (the green patch in Figure 8b) exhibited a high CWP because of its low ETa and high yield. However, the northern corner of the alfalfa fields (the blue patch in Figure 8a), in spite of having a low ETa, exhibited a low CWP as a result of its low yield and inadequate water, as displayed by the RET map. Similarly, the high-water use alfalfa fields (RET > 1) in the eastern regions, with moderate-to-high CWPs, also had moderate-to-high levels of ETa and yield. This suggests that these fields are compensated by high yields resulting in high CWP, despite having more than the required water use. The overall results imply that the factors by which CWP is influenced vary widely in the study area, and there should be careful consideration before making any management decisions on enhancing CWP.

4.5. Analysis on the Scope of Water Conservation

The high CV of CWP for both alfalfa and sugar beet fields implies that by narrowing the variability, there is a wide scope of CWP improvement. CWP enhancement can be achieved either by increasing the yield or maintaining the same yield while reducing the water use [34]. Because yield increment takes time [31], the second option could be more viable in areas where water availability is limited.

In order to better understand the scope of water conservation through CWP improvement, random points were generated from a corresponding spatial map, and scatter plots were prepared among the CWP, yield and ETa in order to observe the association between them (Figure 9). Figure 9a indicates that the distribution range of the alfalfa ETa with yield was high for ETa in the range 500 mm to 1500 mm. However, it is observed that, for ETas above 1500 mm, the variation decreases, and the yield remains constantly high (Figure 9a; rectangular box). This implies that above this range, the reduction of the irrigation water amount would not affect the yield significantly, and its effect would not be adverse. Similar results were observed for sugar beets in the range of ETas from 1200 mm to 1600 mm (Figure 9c; rectangular box), where the yield distribution with ETa was low. The relationship between the CWP and ETa for both crops, alfalfa (Figure 9b) and sugar beet (Figure 9d), showed that the CWP decreases as the ET increases primarily for ETas above 1500 mm for alfalfa and 1200 mm for sugar beet. Therefore, by decreasing the water use above the aforementioned ranges to around 1500 mm and 1200 mm for alfalfa and sugar beet, respectively, we identified a scope of CWP enhancement that keeps the yield constant. Table 4 shows the possible volume of water that could be conserved through CWP enhancement. The results imply that it is possible to save approximately 44.52M cu. m (36,000 acre-ft) of irrigation water volume by reducing the ETa to a range where the yield is not adversely affected and the CWP is enhanced.

Table 4. Possible water saving opportunities by reducing the ETa without adversely affecting the yield.

Alfalfa	
No. of pixels > 1500 mm	214,020
Volume for ETa > 1500 mm	327.73M cu.m
Volume after reducing ETa = 1500 mm	288.92M cu.m
Saved water volume =	38.37M cu.m
Sugar beet	
No. of pixels > 1200 mm	45,357
Volume for ETa > 1200 mm	55.12M cu.m
Volume after reducing ETa = 1200 mm	48.98M cu.m
Saved water volume =	6.14M cu.m
Total volume that can be saved =	44.52M cu.m

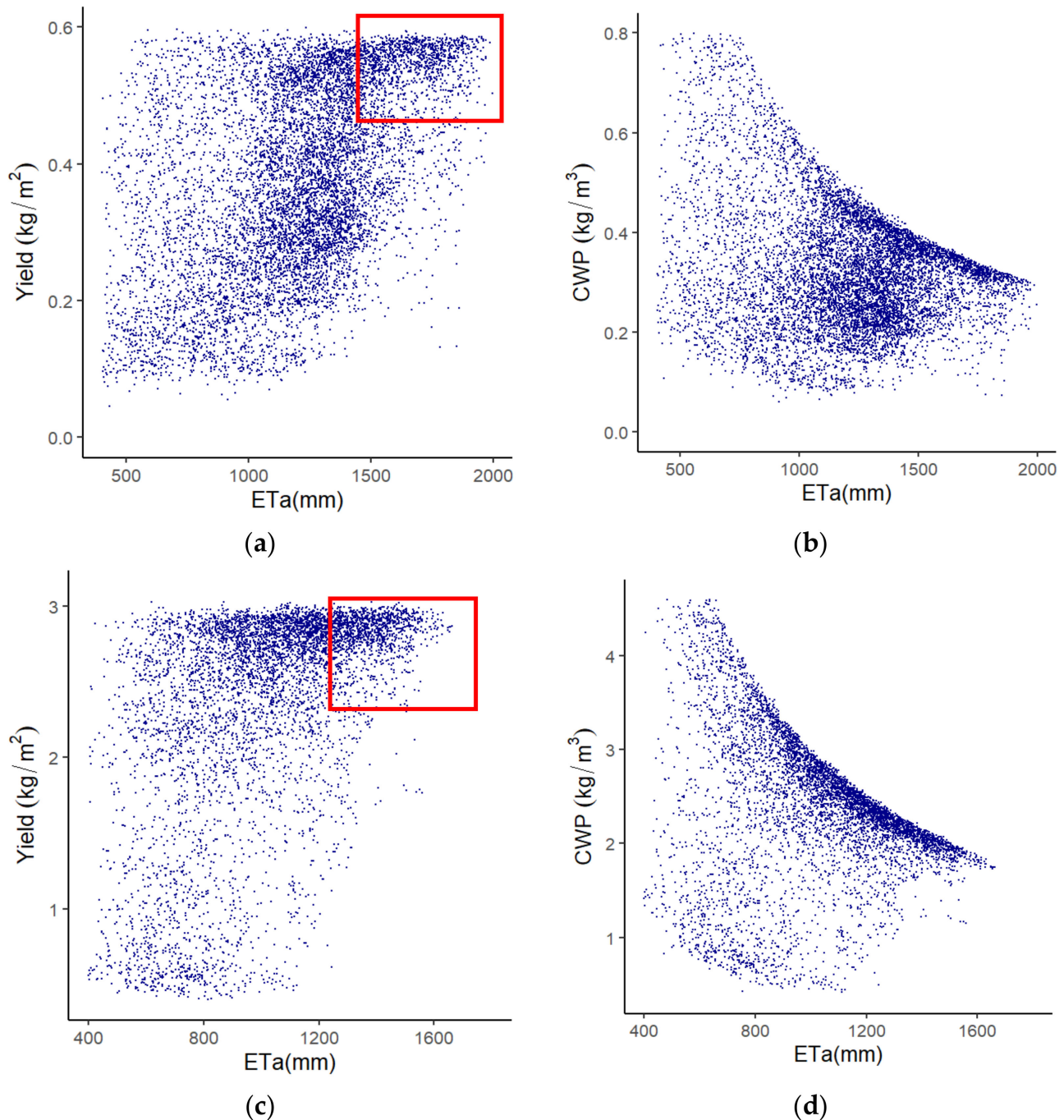


Figure 9. Relationship between (a,c) yield (kg/m²) and ETa (mm), and (b,d) CWP (kg/m³) and ETa (mm) for alfalfa (top row) and sugar beet (bottom row), respectively. The rectangular red box denotes the area where the yield is nearly constant.

Other than water conservation through CWP enhancement, we also identified high-water-use fields through RET analysis. For nearly 32% of alfalfa and 12% of sugar beet pixels with $RET > 1$, the water overuse was equivalent to approximately 11M cu. m (8940 acre-ft) collectively for the two crops. Hence, possible water saving opportunities were also identified for high RET fields, and the spatial map presented in this study helps identify those fields.

5. Discussions

The high yield fluctuation with ET_a found in this analysis is consistent with the previous research findings. [1] found a high variation of irrigated crop yields, including sugar beets, even when the ET_a is constant. Similar high fluxes of alfalfa yield with ET_c were observed by [7] for irrigated land in the Californian desert. The inconsistent relationship of the yield with ET_a below 1500 mm for alfalfa and 1200 mm for sugar beet infers that the yield is only marginally limited by water consumption for both crops beneath this range. This suggests that there are a number of other important factors that influence crop production and, as a result, yield variability. Those factors may include the irrigation and management practices, as well as the soil, nutrients, water table depth, land preparation and fertilizer application, along with the tolerance capacity of the crop itself for drought and salinity [34,35]. In addition, Smeal et al. discussed the dependence of the alfalfa yield on the cutting number and the accumulated growing day temperatures [80]. Therefore, the challenge associated with enhancing CWP in IV by decreasing the ET_a for these ranges would be to maintain a constant yield. Another option would be to reduce the ET in low-yielding fields. This could be a suitable strategy specifically for the IV, where water costs only account 10–20% of the overall alfalfa production costs [7]. Hence, the implementation of water conservation approaches that will result in a greater loss of the hay yield may be undesirable to growers. However, the research may necessitate data from multiple years in order to validate the findings and establish accurate CWP benchmarks.

Although the average spatial variability of the water use within the fields was reasonable for both crops, the use of the average performance value may not inform us about the actual system performance level [77]. Having about 35% of fields with CVws greater than optimal implies spatially heterogeneous water consumption in these fields. Moreover, the high Cva exhibited among the fields implies significant room for improvement in performance among the farmers. Because of the variable growing season, this heterogeneity might represent the somewhat-upper limit for alfalfa. The high variance or non-uniformity does not necessarily imply poor management in all of the fields, as it may also relate to sub-optimal crop husbandry or deficit irrigation practices [74]. Remote sensing alone may not explain the variation. However, the assessment of the variability offered by the distributed nature of the remote sensing aided in locating the non-uniform fields, where further investigation can be performed. Besides fields with water overuse ($RET > 1$), equal attention should be placed on the fields where adequacy is less than optimal ($RET < 1$). A less salt-tolerant alfalfa crop may be unfavorably affected by salinity accumulations due to the reduced water [81] in comparison to moderately salt-tolerant sugar beets.

Using EEFlux to estimate the water usage in this study provided a valuable method for the quantification of the irrigation system performance at both the crop and field levels. The overall accuracy of the ET_a , when compared to the values in the literature, was found to be reasonable. Though the comparison with the kc- ET_o -derived ET_c for several growth stages resulted in differences, the discrepancies may be associated with methodological differences in computing the kc [48,49]. EEFlux considers the current conditions of the satellite overpass time, whereas the reported kc values are the average kc during the growing phases. In addition, although an attempt was made to reduce the large temporal gaps between the image dates by including Landsat 7/8 images, images were unusable for December due to high cloud cover. The gap between the images might have impacted the interpolation results, and ultimately the seasonal ET_a values [62]. The advantage of an eight-day satellite overpass frequency, in comparison to 16 days, to predict the seasonal ET of a cotton crop was observed by [82]. Similarly, we employed a linear interpolation method to generate daily ET_a maps. Previous studies have shown that the use of spline interpolation may improve the seasonal ET_a estimation, although the results were not statistically significant in either case [47].

This study utilized a yield disaggregation method [31] to map the large-scale yield, using county production statistics and NDVI at specific growth stages. The method links the publicly available district-level statistics to remotely sensed data and helps fill the

gap between the two. Because this method avoids complex land surface processes and biophysical parameter estimation [31,37], agricultural managers can map the yields of large areas efficiently. Although pixel-level validation was not performed in this study, the reasonable accuracy from this method in other studies for wheat [31] and rice [37] provides a confidence in others crops as well. Very few studies have explored the use of NDVI in the prediction of the yields of alfalfa and sugar beet in the past. However, in other crops of medium-to-high canopy sizes, such as corn, soybeans and winter wheat, NDVI showed a good correlation with the cropped biomass per area [83,84]. This may also imply that NDVI is a good metric for the estimation of the biomass in the crops analyzed in this study. The uncertainty in the exact growing cycles of the crops may have resulted some bias in the predicted yield using a single NDVI image, which could be improved in future studies by incorporating accurate field data. Nevertheless, the yield disaggregation method using NDVI is a promising approach that brings simplicity to the crop-yield mapping of large areas.

6. Conclusions

In this study, we computed irrigation performance indicators based on equity, adequacy and water productivity, using remote sensing, NDVI and crop production statistics. All of the available Landsat 7/8 images with low cloud cover were processed in the EEFlux platform to obtain ETrf images of the IV. Linear interpolation was performed in order to obtain daily ETrf images. Seasonal ETa images were produced as a sum of the product of the daily ETrf and ETr. Crop classification was performed using S2 images and the RF algorithm, and crop-specific (alfalfa and sugar beet) ETa images were produced for the growing season by a crop map overlay. We computed the WCU as a measure of irrigation equity, RET as a measure of adequacy, and crop water productivity to reflect on productivity. The relationship between the crop ETa, yield and CWP was also studied in brief, in order to identify the scope of the CWP enhancement and water conservation.

The average WCUs for both crops were found to be uniform; however, spatial variation within the fields showed that 36.14% of the sugar beet and 34.17% of the alfalfa fields had variabilities greater than 10%. Similarly, the among-field variability was approximately 19% for both. The variability within and among the fields implies the variation in irrigation and management practices among the farmers and indicates a wide scope for improvement. Another indicator, RET, showed that more than half of the fields were provided with adequate water ($RET > 0.75$). However, about 31.5% of the alfalfa and 12% of the sugar beets were consuming more water than necessary ($RET > 1$), and are therefore where the water conservation should be focused. The results showed that nearly 11M cu. m (8940 acre-ft) of water can be saved by reducing the water overuse in these fields. The CWP showed a wide variation, with a CV of 32.92% for alfalfa and 25.4% for sugar beets, indicating a significant scope for CWP enhancement. Nearly 44.52M cu. m (36,000 acre-ft) of water saving opportunities were identified by reducing the ETa to approximately 1500 mm for alfalfa and 1200 mm for sugar beet, which will enhance the CWP without reducing the yield.

The EEFlux served as a valuable source to compute the ET in a simple and inefficient manner. The MAD and RE, when the mean EEFlux ETa was compared with point representative values from the literature, were as low as 46.43 mm and 0.07, respectively, for alfalfa. Similarly, for sugar beets, the lowest MAD was 0.02. However, it is understood that the EEFlux-computed ETa shows a significant difference with the ETc computed using kc-ETo methods. This may be partly attributed to the methodological difference associated with kc calculation between the two methods. The large gap between the image dates for some months may also have affected the results of the seasonal ETa. The accuracy of ETa mapping is imperative for the accurate estimation of the performance indicators. Further investigation of other interpolation methods, the use of all of the available Landsat images for the growing season, and validation with the ground truth data is recommended for future studies.

Overall, the results of this study confirm the wide scope of water conservation in the valley. Fields with non-uniform irrigation distribution and high RET were visually identified. Similarly, fields with a wide variation in CWP were also predicted, in which—by narrowing the variability—significant CWP enhancement can be achieved. Although the procedure did not provide thorough insight into the reasons for the high variation or high–low values, the bigger picture of irrigation performance across the irrigation district was shown. Policymakers and water authorities may use this information to increase the effectiveness of the water conservation in the IV, which is of primary concern these days.

Author Contributions: Conceptualization, H.S. and S.A.; methodology, U.P.; software, U.P.; validation, U.P., S.A. and H.S.; formal analysis, U.P.; investigation, U.P.; resources, S.A. and H.S.; data curation, U.P.; writing—original draft preparation, U.P.; writing—review and editing, S.A. and H.S.; visualization, U.P.; supervision, H.S. and S.A.; project administration, H.S. and S.A.; funding acquisition, H.S. and S.A. All authors have read and agreed to the published version of the manuscript.

Funding: This research received no external funding.

Institutional Review Board Statement: Not applicable.

Informed Consent Statement: The study did not involve humans.

Data Availability Statement: The data is available upon request.

Conflicts of Interest: The authors declare no conflict of interest.

References

- González-Dugo, M.P.; Mateos, L. Spectral vegetation indices for benchmarking water productivity of irrigated cotton and sugarbeet crops. *Agric. Water Manag.* **2008**, *95*, 48–58. [[CrossRef](#)]
- Taghvaeian, S.; Neale, C.M.; Osterberg, J.C.; Sritharan, S.I.; Watts, D.R. Remote sensing and GIS techniques for assessing irrigation performance: Case study in Southern California. *J. Irrig. Drain. Eng.* **2018**, *144*, 05018002. [[CrossRef](#)]
- Dawadi, S.; Ahmad, S. Changing climatic conditions in the Colorado River Basin: Implications for water resources management. *J. Hydrol.* **2012**, *430*, 127–141. [[CrossRef](#)]
- Kalra, A.; Sagarika, S.; Pathak, P.; Ahmad, S. Hydro-climatological changes in the Colorado River Basin over a century. *Hydrol. Sci. J.* **2017**. [[CrossRef](#)]
- Rahaman, M.M.; Thakur, B.; Kalra, A.; Ahmad, S. Modeling of GRACE-Derived Groundwater Information in the Colorado River Basin. *Hydrology* **2019**, *6*, 19. [[CrossRef](#)]
- Tamaddun, K.; Kalra, A.; Kumar, S.; Ahmad, S. CMIP5 Models' Ability to Capture Observed Trends under the Influence of Shifts and Persistence: An In-depth Study on the Colorado River Basin. *J. Appl. Meteorol. Climatol.* **2019**. [[CrossRef](#)]
- Bali, K.M.; Grismer, M.E.; Tod, I.C. Reduced-runoff irrigation of alfalfa in Imperial Valley, California. *J. Irrig. Drain. Eng.* **2001**, *127*, 123–130. [[CrossRef](#)]
- Sagarika, S.; Kalra, A.; Ahmad, S. Evaluating the effect of persistence on long-term trends and analyzing step changes in streamflows of the continental United States. *J. Hydrol.* **2014**, *517*, 36–53. [[CrossRef](#)]
- Ghumman, A.R.; Ahmad, S.; Khan, R.A.; Hashmi, H.N. Comparative Evaluation of Implementing Participatory Irrigation Management in Punjab Pakistan. *Irrig. Drain.* **2014**, *63*, 315–327. [[CrossRef](#)]
- Dawadi, S.; Ahmad, S. Evaluating the Impact of Demand-Side Management on Water Resources under Changing Climatic Conditions and Increasing Population. *J. Environ. Manag.* **2013**, *114*, 261–275. [[CrossRef](#)]
- Saher, R.; Stephen, H.; Ahmad, S. Understanding the summertime warming in canyon and non-canyon surfaces. *Urban Clim.* **2021**. [[CrossRef](#)]
- Bukhary, S.; Batista, J.; Ahmad, S. Analyzing Land and Water Requirements for Solar Deployment in the Southwestern United States. *Renew. Sustain. Energy Rev.* **2018**, *82*, 3288–3305. [[CrossRef](#)]
- Qaiser, K.; Ahmad, S.; Johnson, W.; Batista, J.R. Evaluating the impact of water conservation on fate of outdoor water use: A study in an arid region. *J. Environ. Manag.* **2011**, *92*, 2061–2068. [[CrossRef](#)]
- Qaiser, K.; Ahmad, S.; Johnson, W.; Batista, J.R. Evaluating Water Conservation and Reuse Policies using a Dynamic Water Balance Model. *Environ. Manag.* **2013**, *51*, 449–458. [[CrossRef](#)] [[PubMed](#)]
- Ghumman, A.R.; Iqbal, M.; Ahmad, S.; Hashmi, H.N. Experimental and Numerical Investigations for Optimal Emitter Spacing in Drip Irrigation. *Irrig. Drain.* **2018**, *67*, 724–737. [[CrossRef](#)]
- Tamaddun, K.; Kalra, A.; Ahmad, S. Potential of rooftop rainwater harvesting to meet outdoor water demand in arid regions. *J. Arid Land.* **2018**, *10*, 68–83. [[CrossRef](#)]
- Ahmad, M.U.D.; Turrall, H.; Nazeer, A. Diagnosing irrigation performance and water productivity through satellite remote sensing and secondary data in a large irrigation system of Pakistan. *Agric. Water Manag.* **2009**, *96*, 551–564. [[CrossRef](#)]

18. Bastiaanssen, W.G.; Bos, M.G. Irrigation performance indicators based on remotely sensed data: A review of literature. *Irrig. Drain. Syst.* **1999**, *13*, 291–311. [[CrossRef](#)]
19. Murray-Rust, H.; Snellen, W.B. *Irrigation System Performance Assessment and Diagnosis*; IWMI: Anand, India, 1993.
20. Menenti, M.; Visser, T.; Morabito, J.A.; Drovandi, A. *Appraisal of Irrigation Performance with Satellite Data and Georeferenced Information: The Rio Tunuyan Irrigation Scheme*; Institute of Irrigation Studies, Southampton University: Southampton, UK, 1989.
21. Moran, M.S. Irrigation management in Arizona using satellites and airplanes. *Irrig. Sci.* **1994**, *15*, 35–44. [[CrossRef](#)]
22. Bastiaanssen, W.G.; Van der Wal, T.; Visser, T.N.M. Diagnosis of regional evaporation by remote sensing to support irrigation performance assessment. *Irrig. Drain. Syst.* **1996**, *10*, 1–23. [[CrossRef](#)]
23. Roerink, G.J.; Bastiaanssen, W.G.; Chambouleyron, J.; Menenti, M. Relating crop water consumption to irrigation water supply by remote sensing. *Water Resour. Manag.* **1997**, *11*, 445–465. [[CrossRef](#)]
24. Alexandridis, T.; Asif, S.; Ali, S. *Water Performance Indicators Using Satellite Imagery for the Fordwah Eastern Sadiqia (South) Irrigation and Drainage Project*; No. H024895; International Water Management Institute: Colombo, Sri Lanka, 1999.
25. Bastiaanssen, W.G.M.; Thiruvengadachari, S.; Sakthivadivel, R.; Molden, D.J. Satellite remote sensing for estimating productivities of land and water. *Int. J. Water Resour. Dev.* **1999**, *15*, 181–186. [[CrossRef](#)]
26. Thiruvengadachari, S.; Sakthivadivel, R. *Satellite Remote Sensing Techniques to Aid Irrigation System Performance Assessment: A Case study in India*; Research Report 09; International Water Management Institute: Colombo, Sri Lanka, 1997; p. 31.
27. Ambast, S.K.; Singh, O.P.; Tyagi, N.K.; Menenti, M.; Roerink, G.J.; Bastiaanssen, W.G.M. Appraisal of irrigation system performance in saline irrigated command using SRS and GIS. In *Operational remote sensing for sustainable development*; Balkema: Rotterdam, The Netherlands, 1999; pp. 457–461.
28. Karatas, B.S.; Akkuzu, E.; Unal, H.B.; Asik, S.; Avci, M. Using satellite remote sensing to assess irrigation performance in Water User Associations in the Lower Gediz Basin, Turkey. *Agric. Water Manag.* **2009**, *96*, 982–990. [[CrossRef](#)]
29. Kharrou, M.H.; Le Page, M.; Chehbouni, A.; Simonneaux, V.; Er-Raki, S.; Jarlan, L.; Chehbouni, G. Assessment of equity and adequacy of water delivery in irrigation systems using remote sensing-based indicators in semi-arid region, Morocco. *Water Resour. Manag.* **2013**, *27*, 4697–4714. [[CrossRef](#)]
30. Geerts, S.; Raes, D. Deficit irrigation as an on-farm strategy to maximize crop water productivity in dry areas. *Agric. Water Manag.* **2009**, *96*, 1275–1284. [[CrossRef](#)]
31. Cai, X.L.; Sharma, B.R. Integrating remote sensing, census, and weather data for an assessment of rice yield, water consumption and water productivity in the Indo-Gangetic River basin. *Agric. Water Manag.* **2010**, *97*, 309–316. [[CrossRef](#)]
32. Immerzeel, W.W.; Gaur, A.; Zwart, S.J. Integrating remote sensing and a process-based hydrological model to evaluate water use and productivity in a south Indian catchment. *Agric. Water Manag.* **2008**, *95*, 11–24. [[CrossRef](#)]
33. Yan, N.; Wu, B. Integrated spatial–temporal analysis of crop water productivity of winter wheat in Hai Basin. *Agric. Water Manag.* **2014**, *133*, 24–33. [[CrossRef](#)]
34. Zwart, S.J.; Bastiaanssen, W.G. SEBAL for detecting spatial variation of water productivity and scope for improvement in eight irrigated wheat systems. *Agric. Water Manag.* **2007**, *89*, 287–296. [[CrossRef](#)]
35. Ahmed, B.M.; Tanakamaru, H.; Tada, A. Application of remote sensing for estimating crop water requirements, yield, and water productivity of wheat in the Gezira Scheme. *Int. J. Remote Sens.* **2010**, *31*, 4281–4294. [[CrossRef](#)]
36. Gorantiwar, S.D.; Smout, I.K. Performance assessment of irrigation water management of heterogeneous irrigation schemes: 1. A framework for evaluation. *Irrig. Drain. Syst.* **2005**, *19*, 1–36. [[CrossRef](#)]
37. Usman, M.; Liedl, R.; Shahid, M.A. Managing irrigation water by yield and water productivity assessment of a rice-wheat system using remote sensing. *J. Irrig. Drain. Eng.* **2014**, *140*, 04014022. [[CrossRef](#)]
38. Saher, R.; Stephen, H.; Ahmad, S. Urban evapotranspiration of Green Spaces in Arid Regions through Two Established Approaches: A Review of Key Drivers, Advancements, Limitations, and Potential Opportunities. *Urban Water J.* **2020**. [[CrossRef](#)]
39. Zhang, K.; Kimball, J.S.; Running, S.W. A review of remote sensing based actual evapotranspiration estimation. *Wiley Interdiscip. Rev. Water* **2016**, *3*, 834–853. [[CrossRef](#)]
40. Kustas, W.P.; Norman, J.M. Use of remote sensing for evapotranspiration monitoring over land surfaces. *Hydrol. Sci. J.* **1996**, *41*, 495–516. [[CrossRef](#)]
41. Reyes-González, A.; Kjaersgaard, J.; Trooien, T.; Hay, C.; Ahiablame, L. Estimation of crop evapotranspiration using satellite remote sensing-based vegetation index. *Adv. Meteorol.* **2018**, 4525021. [[CrossRef](#)]
42. Er-Raki, S.; Chehbouni, A.; Duchemin, B. Combining satellite remote sensing data with the FAO-56 dual approach for water use mapping in irrigated wheat fields of a semi-arid region. *Remote Sens.* **2010**, *2*, 375–387. [[CrossRef](#)]
43. Bastiaanssen, W.G.; Menenti, M.; Feddes, R.A.; Holtslag, A.A.M. A remote sensing surface energy balance algorithm for land (SEBAL). 1. Formulation. *J. Hydrol.* **1998**, *212*, 198–212. [[CrossRef](#)]
44. Allen, R.G.; Tasumi, M.; Trezza, R. Satellite-based energy balance for mapping evapotranspiration with internalized calibration (METRIC)—Model. *J. Irrig. Drain. Eng.* **2007**, *133*, 380–394. [[CrossRef](#)]
45. Roerink, G.J.; Su, Z.; Menenti, M. S-SEBI: A simple remote sensing algorithm to estimate the surface energy balance. *Phys. Chem. Earth B* **2000**, *25*, 147–157. [[CrossRef](#)]
46. Singh, R.K.; Senay, G.B. Comparison of four different energy balance models for estimating evapotranspiration in the Midwestern United States. *Water* **2016**, *8*, 9. [[CrossRef](#)]

47. Singh, R.K.; Liu, S.; Tieszen, L.L.; Suyker, A.E.; Verma, S.B. Estimating seasonal evapotranspiration from temporal satellite images. *Irrig. Sci.* **2012**, *30*, 303–313. [CrossRef]
48. De Oliveira Costa, J.; José, J.V.; Wolff, W.; de Oliveira, N.P.R.; Oliveira, R.C.; Ribeiro, N.L.; Coelho, R.D.; da Silva, T.J.A.; Silva, E.M.B.; Schlichting, A.F. Spatial variability quantification of maize water consumption based on Google EEflux tool. *Agric. Water Manag.* **2020**, *232*, 106037. [CrossRef]
49. Venancio, L.P.; Eugenio, F.C.; Filgueiras, R.; França da Cunha, F.; Argolo dos Santos, R.; Ribeiro, W.R.; Mantovani, E.C. Mapping within-field variability of soybean evapotranspiration and crop coefficient using the Earth Engine Evaporation Flux (EEFlux) application. *PLoS ONE* **2020**, *15*, e0235620. [CrossRef] [PubMed]
50. Lambert, M.J.; Traoré, P.C.S.; Blaes, X.; Baret, P.; Defourny, P. Estimating smallholder crops production at village level from Sentinel-2 time series in Mali's cotton belt. *Remote Sens. Environ.* **2018**, *216*, 647–657. [CrossRef]
51. Kayad, A.; Sozzi, M.; Gatto, S.; Marinello, F.; Pirotti, F. Monitoring within-field variability of corn yield using Sentinel-2 and machine learning techniques. *Remote Sens.* **2019**, *11*, 2873. [CrossRef]
52. Morel, J.; Todoroff, P.; Bégué, A.; Bury, A.; Martiné, J.F.; Petit, M. Toward a satellite-based system of sugarcane yield estimation and forecasting in smallholder farming conditions: A case study on Reunion Island. *Remote Sens.* **2014**, *6*, 6620–6635. [CrossRef]
53. Sibley, A.M.; Grassini, P.; Thomas, N.E.; Cassman, K.G.; Lobell, D.B. Testing remote sensing approaches for assessing yield variability among maize fields. *Agron. J.* **2014**, *106*, 24–32. [CrossRef]
54. Shanahan, J.F.; Schepers, J.S.; Francis, D.D.; Varvel, G.E.; Wilhelm, W.W.; Tringe, J.M.; Major, D.J. Use of remote-sensing imagery to estimate corn grain yield. *Agron. J.* **2001**, *93*, 583–589. [CrossRef]
55. Tucker, C.J.; Holben, B.N.; Elgin, J.H., Jr.; McMurtrey, J.E., III. Relationship of spectral data to grain yield variation [within a winter wheat field]. *Photogramm. Eng. Remote Sens.* **1980**, *46*, 657–666.
56. Shirsath, P.B.; Sehgal, V.K.; Aggarwal, P.K. Downscaling regional crop yields to local scale using remote sensing. *Agriculture* **2020**, *10*, 58. [CrossRef]
57. Imperial County Planning and Development Services. Agriculture Element. 2015. Available online: <https://www.icpds.com/assets/planning/agricultural-element-2015.pdf> (accessed on 12 July 2020).
58. Inouye, D. Crop Water Requirements Imperial Valley. 1981. Available online: <https://nrm.dfg.ca.gov/FileHandler.ashx?DocumentID=7226> (accessed on 12 July 2020).
59. Kayad, A.G.; Al-Gaadi, K.A.; Tola, E.; Madugundu, R.; Zeyada, A.M.; Kalaitzidis, C. Assessing the spatial variability of alfalfa yield using satellite imagery and ground-based data. *PLoS ONE* **2016**, *11*, e0157166. [CrossRef]
60. Allen, R.G.; Pereira, L.S.; Raes, D.; Smith, M. Crop Evapotranspiration-Guidelines for computing crop water requirements-FAO Irrigation and drainage paper 56. *FAO Rome* **1998**, *300*, D05109.
61. Pruitt, W.O.; Doorenbos, J. *Empirical Calibration: A Requisite for Evapotranspiration Formulae Based on Daily or Longer Mean Climate Data?* Hungarian National Committee: Budapest, Hungary, 1977.
62. Salgado, R.; Mateos, L. Evaluation of different methods of estimating ET for the performance assessment of irrigation schemes. *Agric. Water Manag.* **2021**, *243*, 106450. [CrossRef]
63. Hanson, B.; Putnam, D.; Snyder, R. Deficit irrigation of alfalfa as a strategy for providing water for water-short areas. *Agric. Water Manag.* **2007**, *93*, 73–80. [CrossRef]
64. Wright, J.L. New evapotranspiration crop coefficients. *J. Irrig. Drain. Div.* **1982**, *108*, 57–74. [CrossRef]
65. Pruitt, W.O.; Lourence, F.; Von Oettingen, S. Water use by crops as affected by climate and plant factors. *Calif. Agric.* **1972**, *26*, 10–14.
66. Walter, I.A.; Allen, R.G.; Elliott, R.; Jensen, M.E.; Itenfisu, D.; Mecham, B.; Martin, D. ASCE's standardized reference evapotranspiration equation. In *Watershed Management and Operations Management*; American Society of Civil Engineers: Reston, VA, USA, 2000; pp. 1–11.
67. Allen, R.G.; Clemmens, A.J.; Burt, C.M.; Solomon, K.; O'Halloran, T. Prediction accuracy for projectwide evapotranspiration using crop coefficients and reference evapotranspiration. *J. Irrig. Drain. Eng.* **2005**, *131*, 24–36. [CrossRef]
68. Bos, M.G.; Burton, M.A.; Molden, D.J. *Irrigation and Drainage Performance Assessment: Practical Guidelines*; CABI Publishing: Oxford, UK, 2005.
69. Blatchford, M.L.; Mannaerts, C.M.; Zeng, Y.; Nouri, H.; Karimi, P. Status of accuracy in remotely sensed and in-situ agricultural water productivity estimates: A review. *Remote Sens. Environ.* **2019**, *234*, 111413. [CrossRef]
70. Bhattarai, N.; Shaw, S.B.; Quackenbush, L.J.; Im, J.; Niraula, R. Evaluating five remote sensing based single-source surface energy balance models for estimating daily evapotranspiration in a humid subtropical climate. *Int. J. Appl. Earth Obs. Geoinf.* **2016**, *49*, 75–86. [CrossRef]
71. José, J.V.; Oliveira, N.P.R.D.; Silva, T.J.D.A.D.; Bonfim-Silva, E.M.; Costa, J.D.O.; Fenner, W.; Coelho, R.D. Quantification of cotton water consumption by remote sensing. *Geocarto Int.* **2020**, *35*, 1800–1813. [CrossRef]
72. Costa, J.D.O.; Coelho, R.D.; Wolff, W.; José, J.V.; Folegatti, M.V.; Ferraz, S.F.D.B. Spatial variability of coffee plant water consumption based on the SEBAL algorithm. *Sci. Agric.* **2019**, *76*, 93–101. [CrossRef]
73. Kamble, B.; Kilic, A.; Hubbard, K. Estimating crop coefficients using remote sensing-based vegetation index. *Remote Sens.* **2013**, *5*, 1588–1602. [CrossRef]
74. Santos, C.; Lorite, I.J.; Tasumi, M.; Allen, R.G.; Fereres, E. Integrating satellite-based evapotranspiration with simulation models for irrigation management at the scheme level. *Irrig. Sci.* **2008**, *26*, 277–288. [CrossRef]

75. Molden, D.J.; Gates, T.K. Performance measures for evaluation of irrigation-water-delivery systems. *J. Irrig. Drain. Eng.* **1990**, *116*, 804–823. [[CrossRef](#)]
76. Inouye, D.; Yoha, R.E. Preliminary Evaluation of Soils and Irrigation Practices in the Imperial Valley. 1981. Available online: <https://nrm.dfg.ca.gov/FileHandler.ashx?DocumentID=9024> (accessed on 19 November 2020).
77. Bastiaanssen, W.G.M.; Brito, R.A.L.; Bos, M.G.; Souza, R.A.; Cavalcanti, E.B.; Bakker, M.M. Low-cost satellite data for monthly irrigation performance monitoring: Benchmarks from Nilo Coelho, Brazil. *Irrig. Drain. Syst.* **2001**, *15*, 53–79. [[CrossRef](#)]
78. Patil, V.C.; Al-Gaadi, K.A.; Madugundu, R.; Tola, E.H.; Marey, S.; Aldosari, A.; Gowda, P.H. Assessing agricultural water productivity in desert farming system of Saudi Arabia. *IEEE J. Sel. Top. Appl. Earth Obs. Remote Sens.* **2014**, *8*, 284–297. [[CrossRef](#)]
79. Madugundu, R.; Al-Gaadi, K.A.; Tola, E.; Patil, V.C.; Biradar, C.M. Quantification of agricultural water productivity at field scale and its implication in on-farm water management. *J. Indian Soc. Remote Sens.* **2017**, *45*, 643–656. [[CrossRef](#)]
80. Smeal, D.; Kallsen, C.E.; Sammis, T.W. Alfalfa yields as related to transpiration, growth stage and environment. *Irrig. Sci.* **1991**, *12*, 79–86. [[CrossRef](#)]
81. Maas, E.V.; Hoffman, G.J. Crop salt tolerance—Current assessment. *J. Irrig. Drain. Div.* **1977**, *103*, 115–134. [[CrossRef](#)]
82. French, A.N.; Hunsaker, D.J.; Thorp, K.R. Remote sensing of evapotranspiration over cotton using the TSEB and METRIC energy balance models. *Remote Sens. Environ.* **2015**, *158*, 281–294. [[CrossRef](#)]
83. Lokupitiya, E.; Lefsky, M.; Paustian, K. Use of AVHRR NDVI time series and ground-based surveys for estimating county-level crop biomass. *Int. J. Remote Sens.* **2010**, *31*, 141–158. [[CrossRef](#)]
84. Meng, J.; Du, X.; Wu, B. Generation of high spatial and temporal resolution NDVI and its application in crop biomass estimation. *Int. J. Digit. Earth* **2013**, *6*, 203–218. [[CrossRef](#)]